

---

MASTER THESIS

---

# DIGITAL PREDISTORTION OF AN 802.11N WLAN TRANSMITTER

---

conducted at the  
Signal Processing and Speech Communications Laboratory  
Graz University of Technology, Austria

in cooperation with  
FTW Forschungszentrum Telekommunikation Wien GmbH  
Vienna, Austria

by  
Peter Paul Reinprecht

Supervisor:  
Priv.-Doz. Dipl.-Ing. Dr.techn. Christian Vogel

Graz, June, 2013



## Statutory Declaration

I declare that I have authored this thesis independently, that I have not used other than the declared sources/resources, and that I have explicitly marked all material which has been quoted either literally or by content from the used sources.

---

date

---

(signature)



## **Abstract**

Wireless local area network (WLAN) transmitters are designed to transmit data with high data rates using high bandwidths. The transmitted signals are modulated using orthogonal frequency division multiplexing (OFDM) to efficiently cover the whole bandwidth. Due to the parallel transmission of different subcarriers, the signal is a superposition of all separate channels and can have a high peak-to-average power ratio (PAPR) caused by constructive interference. Therefore, the highest signal power level can be much larger than the average power and the power amplifier (PA) can only be used within a certain range to avoid distortions. To increase the performance of existing PAs, digital predistortion is used to compensate for the nonlinear effects, which are caused by saturation and ensure a linear amplification up to the maximal desired output power.

In this thesis, an existing 802.11n WLAN transmitter is analyzed and digital predistortion for linearizing the transmitter is considered. The evaluation of the transmitter includes a detailed study of the individual components of the transmitter and their interaction. It is shown that the nonlinear behavior of the amplifier can be identified and compensated.



## **Kurzfassung**

Sendestationen von drahtlosen lokalen Netzwerken (WLANs) übertragen Daten mit hoher Transferrate und hoher Bandbreite. Zur effizienten Nutzung der Bandbreite wird das Signal mit Hilfe eines orthogonalen Frequenzmultiplexverfahren (OFDM) auf mehrere Träger moduliert. Durch das Zusammenfügen der getrennt voneinander modulierten Teilsignale zu einem Gesamtsignal, kann es durch konstruktive Interferenz zu hohen Leistungsspitzen kommen, die deutlich über der durchschnittlich übertragenen Leistung liegen. Aufgrund der hohen Spitzen kann ein Leistungsverstärker nur in einem bestimmten Aussteuerbereich betrieben werden, damit keine Verzerrungen durch Sättigungserscheinungen auftreten. Um die Effizienz des Verstärkers zu erhöhen, wird das Signal durch eine digitale Vorverzerrung (DPD) so verzerrt, dass die Nichtlinearität des Verstärkers ausgeglichen wird.

In dieser Arbeit wird ein 802.11n WLAN Sender simuliert und mit Hilfe einer DPD linearisiert. Der Sender als Gesamtsystem und alle Einzelkomponenten werden untersucht und evaluiert. Es wird gezeigt, dass das nichtlineare Verhalten des Leistungsverstärkers identifiziert und kompensiert werden kann.



## **Acknowledgement**

I want to thank my family for supporting me during the last few years. Their support made it possible for me to find my own way through my years of study. Further on, I want to thank my friends who always have been there for me whenever I needed distraction or encouragement. I also want to say thank you to my fellow students and my colleagues and friends I worked with in the student union, CISV and BEST. I am grateful for exchanging ideas, realizing projects together, giving me the opportunity to explore the diversity of working in groups and for the great time I spent with all of them.

I owe special thanks to my supervisor Christian Vogel. He guided me through the world of nonlinear signal processing and supported me whenever I got stuck. Thanks also go to my colleagues at FTW here in Graz, but also to those in Vienna. I am thankful for their contributions to the simulation platform, the interesting discussions we had and the pleasant working environment.

This master thesis was written in 2012/2013 at the Signal Processing and Speech Communications Laboratory at Graz University of Technology in cooperation with FTW Forschungszentrum Telekommunikation Wien GmbH.



# Contents

<b>1</b>	<b>Introduction</b>	<b>1</b>
1.1	Motivation . . . . .	1
1.2	Objectives . . . . .	1
1.3	Thesis Overview . . . . .	2
1.4	WLAN Standard . . . . .	2
1.4.1	Modulation . . . . .	2
1.4.2	Transmitter Specifications . . . . .	4
<b>2</b>	<b>System Model</b>	<b>7</b>
2.1	Modeling the Transmitter Path . . . . .	7
2.1.1	Baseband Modeling . . . . .	11
2.1.2	Transmitter Analysis . . . . .	14
2.2	Modeling the Power Amplifier . . . . .	15
2.2.1	Volterra Series . . . . .	15
2.2.2	Memoryless Model . . . . .	17
2.2.3	Memory Polynomial . . . . .	18
2.2.4	Quasi-memoryless Model . . . . .	18
<b>3</b>	<b>Calibration Methods</b>	<b>21</b>
3.1	Preprocessing . . . . .	21
3.2	Used Identification Procedure . . . . .	23
<b>4</b>	<b>Calibration Performance</b>	<b>27</b>
4.1	Quality of the Measurements . . . . .	27
4.1.1	Plots . . . . .	28
4.1.2	Figures of Merit . . . . .	28
4.2	PA Model . . . . .	30
4.3	Idealized Transmitter . . . . .	31
4.3.1	Performance Evaluation . . . . .	31
4.3.2	Ideal Inverse of the PA . . . . .	35
4.3.3	Ideal Compensation of the Pulse Shaping Filter . . . . .	39
4.3.4	Influence of the Look-up Table Size . . . . .	42
4.4	Identification of the Transmitter . . . . .	43

4.5	Identification of the DPD . . . . .	46
4.5.1	Identification of the Inverse Nonlinearity . . . . .	47
4.5.2	Identification of the Inverse Memory . . . . .	48
4.5.3	Identification of the Inverse Transmitter . . . . .	49
4.5.4	Performance of the DPD for High Output Power . . . . .	51
<b>5</b>	<b>Conclusion</b>	<b>55</b>
<b>A</b>	<b>Volterra Models</b>	<b>57</b>

# 1

## Introduction

Next generation wireless local area networks (WLANs) will be designed to allow a higher data throughput by maintaining the frequency bands at 2.4 and 5 GHz. To achieve this goal the bandwidth have to be increased and a higher order modulation have to be used. To ensure a high spectral efficiency, orthogonal frequency division multiplexing (OFDM) is used for the modulation which introduces a high peak-to-average power ratio (PAPR). Due to the high PAPR the power amplifier (PA) can only be operated within a small range which leads to low power efficiency. The larger bandwidth does also effect the requirements of the PA of a WLAN device as memory effects may occur. Another requirement is the optimization of a WLAN device in terms of size and power efficiency which is important especially for mobile communication devices. To sum up, to efficiently handle high PAPR signals, the PA needs to be operated close to or even in saturation which leads to nonlinear distortions.

### 1.1 Motivation

Digital predistortion (DPD) is a popular method to linearize PAs. There are many models and structures which are used to find the DPD. This thesis aims for analyzing a given WLAN transmitter, examine all system components and find the best possible DPD to increase the overall performance of the transmitter.

### 1.2 Objectives

This thesis aims for optimizing a given IEEE 802.11n (802.11n) WLAN transmitter which is given by a hardware radio frequency integrated circuit (RFIC). The goal is to simulate the

transmitter using MathWorks MATLAB<sup>®</sup> (MATLAB) and reduce the error vector magnitude (EVM) for a output power of 17 dBm and 19 dBm. It will be shown that the performance can be increased and the bounds which are given by the transmitter will be elaborated.

### 1.3 Thesis Overview

In the remainder of the introduction the most important definitions which must be considered when dealing with WLAN systems. Then all relevant models which are needed to be considered for the implementation of the system components and the nonlinear behavior are elaborated in Chapter 2. Chapter 3 shows which things have to be considered before the identification can be performed and which algorithm is used for the identification. In the end the given transmitter will be examined in an ideal and an real scenario where the system and the inverse of the system will be identified and evaluated.

### 1.4 WLAN Standard

WLAN is defined by IEEE 802.11 standards, which are created by the *IEEE Working Group for WLAN Standards*<sup>1</sup>. The standard 802.11n allows a high throughput up to 600 Mb/s using a bandwidth of 40 MHz in the 2.4 GHz and the 5 GHz band [1]. Next generations WLANs (802.11ac) must be able to increase the throughput above 1 Gb/s, but do not extend the band above the traditional 6 GHz WLAN band which can be achieved by modifying the 802.11n standard. This section gives an overview on the most important specifications which are needed for the thesis and an outlook to next generation WLANs. Further descriptions can be found in [2, 3].

To ensure the backwards compatibility of the new standard details from the previous standards are re-used. The bandwidth of the channels used in 802.11n [2] are specified with 20 and 40 MHz. IEEE 802.11ac (802.11ac) must support those and an additional 80 MHz channel. To achieve the highest possible throughput there are features like higher bandwidths (160 or 80+80 MHz), the support of higher modulation (256QAM), etc. implemented which can be used optional. By using the mandatory parameter a data rate of  $\sim 293$  Mb/s can be achieved.

#### 1.4.1 Modulation

The wide channels used in WLANs are frequency selective. Due to the short symbol duration which is caused by the high data rate and the frequency selectivity of the channel intersymbol interference (ISI) can occur [4]. To eliminate this effect OFDM is used for WLAN systems [3, 5, 6]. According to OFDM the wide channel is divided into smaller narrow-band channels which can assumed to be flat. A serial to parallel converter split the data into a number of

---

<sup>1</sup> <http://grouper.ieee.org/groups/802/11/>

data streams which are transmitted parallel. Fig. 1.1 illustrates this parallel transmission in the frequency domain.

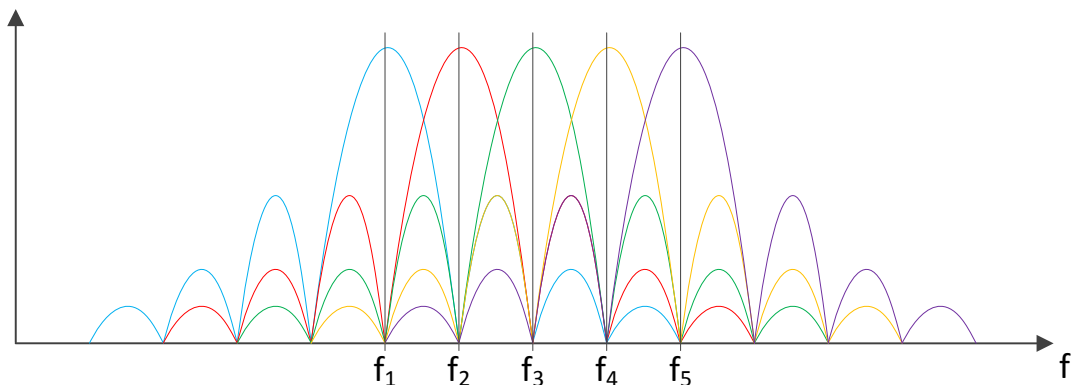


Figure 1.1: Subcarriers of an OFDM signal.

An OFDM symbol can be mathematically expressed in base band as [5]

$$s(t) = \sum_{k=0}^{N-1} s_k \varphi_k(t), \quad \text{for } 0 \leq t \leq T_s \quad (1.1)$$

where  $s_k$  are the  $N$  complex symbols which will be transmitted,

$$\varphi_k(t) = \begin{cases} e^{j2\pi f_k t} & \text{for } 0 \leq t \leq T_s, \\ 0 & \text{otherwise} \end{cases}$$

for  $k = 0, 1, \dots, N - 1$  and  $f_k = f_0 + k\Delta f$ . Further on  $T_s$  is the duration of the OFDM symbol,  $f_0$  is the center frequency and  $\Delta f$  represent the distance between two adjacent subcarriers. The distance between the subcarriers must be high enough to not interfere with each other, which is given by the orthogonality condition  $T_s \Delta f = 1$ .

The total signal length of an OFDM symbol is extended by a guard time  $T_g$  to decrease the influence of delay spread on the wireless channel [4]. The guard time can be either a cyclic prefix, a cyclic suffix or a combination of both and increase the total symbol time to  $T = T_s + T_g$ .

To avoid interferences with adjacent channels the subcarriers on the margin of the channel are used as guard subcarriers and do not transmit information. The subcarriers in the center of the frequency band are called DC subcarriers and are unused to avoid problems during digital/analog and analog/digital conversions. All the subcarriers that are not used for transmission of information are called null subcarriers. A list of the subcarriers for data transmission is shown in Tab. 1.1.

Channel Size	Number of Subcarriers	Subcarriers Transmitting Signal
20 MHz	64	-28 to -1 and 1 to 28
40 MHz	128	-58 to -2 and 2 to 58

Table 1.1: Subcarriers per 11ac transmission bandwidth [2].

### 1.4.2 Transmitter Specifications

#### Spectral Mask

The transmitter of a WLAN device must insure to transmit within a defined spectral mask in order to avoid interchannel interference (ICI). Fig. 1.2 shows the spectral mask which is used in 802.11n. The frequency bounds, which are illustrated as A, B, C and D are specified for all bandwidths in Tab. 1.2.

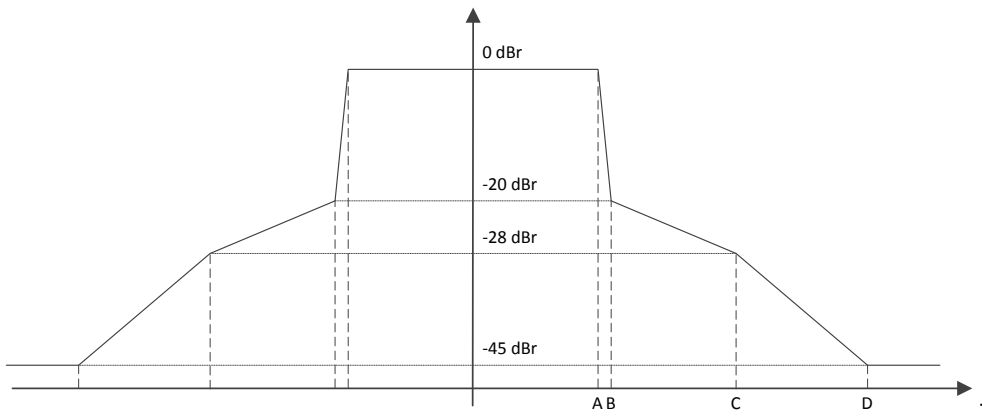


Figure 1.2: Transmit spectral mask definition in 802.11n.

Channel Size	A	B	C	D
20 MHz	9 MHz	11 MHz	20 MHz	30 MHz
40 MHz	19 MHz	21 MHz	40 MHz	60 MHz

Table 1.2: Frequency offsets for spectral requirements [2].

The new standard 802.11ac does not require the high attenuation above point D as the level is reduced to -40 dBm which is discussed in [7].

#### Spectral Flatness

Inside the frequency band the energy of the subcarriers have to stay on a similar power level. Therefore, the average of the subcarriers in the region of the inner subcarriers (Region A) is

calculated. The energy of each subcarrier in 802.11n must lie within  $\pm 2$  dB of the average energy. All the other subcarriers defined in region B must be in the range of  $+2/-4$  dB. Tab. 1.2 shows the allocation of the subcarriers for the two regions. Like the spectral mask also the bounds for

Channel Size	Region A ( $\pm 2$ dB)	Region B ( $+2/-4$ dB)
20 MHz	1 to 16 and -1 to -16	17 to 28 and -17 to -28
40 MHz	2 to 42 and -2 to -42	43 to 58 and -43 to -58

Table 1.3: Bounds for spectral flatness in 801.11n [2].

the spectral flatness are extended in 802.11ac. For region A the bound is  $\pm 4$  dB and  $+4/-6$  dB for region B.

### Output Power

The maximal allowed output power depends on the country where the transmitter is used. The limits for the United States, Europe and Japan are defined in Annex I of [2]. The desired output power of 19 dBm is below the maximal output power for all the country specific regulations and is therefore no longer discussed.

### Relative constellation error

The relative constellation error (RCE) gives the average root mean square (RMS) constellation error of the transmitted signal. It is calculated by averaging the constellation error over the subcarriers, the OFDM frames and the spatial streams whereby the number of spatial streams should be the number of space-time streams [2]. The allowed RCE depends on the modulation and the used coding rate and is defined in Tab. 1.4. A more general form of the RCE is the EVM which will also be used in this thesis and is elaborated in Section 4.1.2 on page 28.

Modulation	Coding rate	RCE
BPSK	1/2	-5
QPSK	1/2	-10
QPSK	3/4	-13
16-QAM	1/2	-16
16-QAM	3/4	-19
64-QAM	2/3	-22
64-QAM	3/4	-25
64-QAM	5/6	-28

Table 1.4: Allowed relative constellation error in 802.11n [2].



## 2

**System Model**

This section shows how the transmitter path can be modeled, shows how simplifications like baseband modeling can be performed and what is needed to close the loop and identify the behavior of the transmitter. Furthermore all relevant methods are introduced how the nonlinearity of the PA can be modeled.

**2.1 Modeling the Transmitter Path**

The purpose of a transmitter is to transform the digital data to an analog waveform, which can be transmitted over a wireless channel. Therefore the output of the transmitter has to be an

- band limited,
- analog signal which is
- modulated to the radio frequency (RF) with
- high power.

A basic structure of such a transmitter is illustrated in Fig. 2.1. The input data, which is a

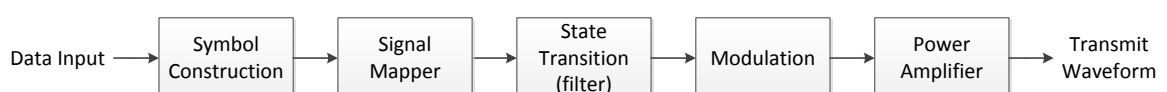


Figure 2.1: Block diagram of a transmitter [8]

bit stream, is first grouped together to symbols by the *Symbol Construction*. Each symbol is transferred to a predefined complex symbol state by the *Signal Mapper* to get complex values. The *State Transition* converts the complex values to an analog band limited signal which will be modulated to the desired carrier frequency by the *Modulation* and amplified by the *Power Amplifier*.

The system model shown in Fig. 2.1 is a general approach and can be rearranged for a more specific WLAN model shown in Fig. 2.2. The enhancement of the second model is that the creation of the signal is combined in one block and the state transition is extended to a chain of signal processing blocks to allow more flexibility and fulfill all specifications.

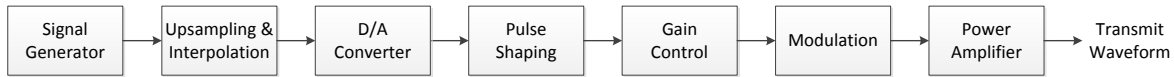


Figure 2.2: Block diagram of a WLAN transmitter

On the next pages every system block will be introduced including the most important effects of this block for the transmitter.

**Signal Generator** The whole process how to generate the OFDM symbol including *Data Generation*, *Symbol Construction*, *Signal Mapping* and the first part of the *State Transition* is combined in one Signal Generator block. This allow to predefine different kind of input data like OFDM Symbols, single tones, multi tones, etc. with pre-defined parameter like the signal rate.

**Upsampling and Interpolation** This block is used to convert the input signal to the required bit rate. A linear phase low pass (LP) finite impulse response (FIR) filter is used for the interpolation.

**Impact** The upsampling produces images in frequency domain which must be filtered by a LP filter to eliminate the influence. Fig. 2.3 illustrate the power spectral density (PSD) of an OFDM input signal on the rate of 80 MHz and the signal after upsampling and interpolation with 240 MHz. As the upsampled signal is used for the reference input, the identification will always try to identify the images of the upsampling as well, even though they do not exist in the output signal any more. Therefore, the performance of the identification can be increased by either using an OFDM signal which is generated on the correct rate or filter the images using another LP filter.

**D/A Converter** The digital to analog converter (DAC) converts the digital signal to the analog signal domain. As MATLAB can only handle digital signals, the analog domain is modeled by high oversampling of the signal which is illustrated in Fig. 2.4.

**Impact** As the DAC does only have a limited amount of bits the output is quantized which can be seen in frequency domain as adding a noise floor. The signal power of the noise floor  $P_N$

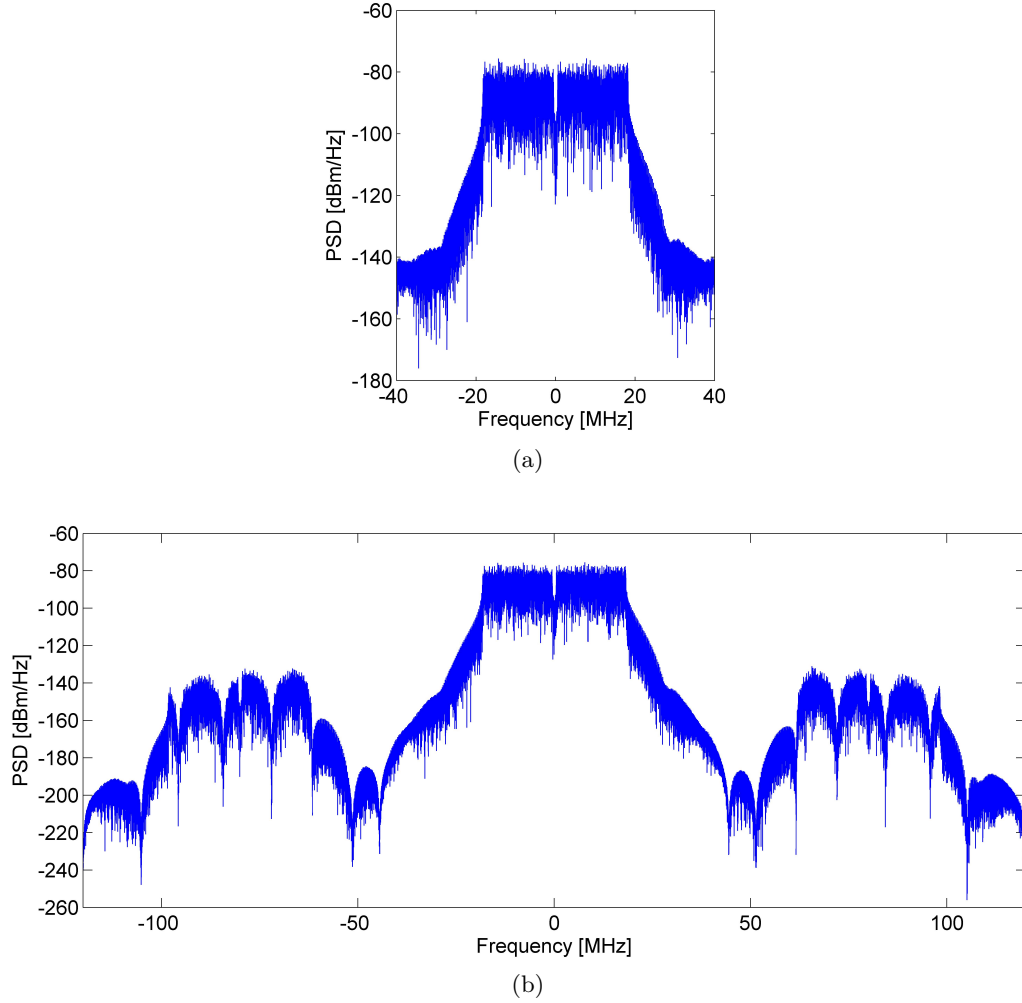


Figure 2.3: PSD of the (a) OFDM signal, (b) upsampled OFDM signal.



Figure 2.4: Block diagram of a DAC

can be determined by

$$P_N = 20 \cdot \log\left(\frac{1}{2^Q}\right) \quad (2.1)$$

where  $Q$  is the number of bits of the quantizer.

**Pulse Shaping** The pulse shaping is realized by a LP filter and is needed to ensure the spectral mask requirements which are given by the WLAN standard (see Section 1.4.2). In many applications the pulse shaping filter is realized before the DAC to allow a simpler filter design. If the pulse shaping is placed in the digital part, the analog part of the transmitter must be

linear enough to ensure not to violate the spectral mask on the output.

**Impact** To fulfill the required specifications the filter must have a steep cutoff. This behavior improves the quality of the output signal of the transmitter without predistortion. As the DPD, which have the task to compensate the nonlinearities of the PA is always in digital domain and therefore in front of the DAC, the pulse shaping filter also cuts the out-of-band components which were created by the DPD to compensate the nonlinearities of the PA. A detailed discussion of this effect can be found in Section 4.3 on page 31.

**Gain Control** An analog gain control is used to allow the reduction of the transmitted power without introducing additional losses due to quantization of the DAC. The gain control can be adjusted from -6 to +8 dB in steps of 2 dB.

**Impact** The different gain settings do directly affect the PA as a higher gain in the gain control leads to a higher compression in the PA and therefore a higher nonlinearity. For the identification it is important to distinguish between the gain before the PA and the gain of the PA to find an accurate model.

**Modulation** The Up-converter modulates the analog signal from the baseband to the high frequency (HF) band. This device does also introduce a configurable gain of -3 and -15 dB. For simple baseband simulations (see Section 2.1.1) the signal does not have to be modulated which reduce this block to a simple gain stage. For simplicity the gain of the up-converter and the gain control can be combined to one gain stage with one pre-gain parameter.

**Power Amplifier** The task of the PA is to amplify the signal to allow the transmission on a wireless channel. An idealized amplitude characteristic of a typical PA is illustrated in Fig. 2.5. To maximize the efficiency, the whole output range must be used which leads to nonlinear distortions. These distortions provoke spectral broadening and must therefore be avoided to not violate the spectral mask (see Section 1.4.2).

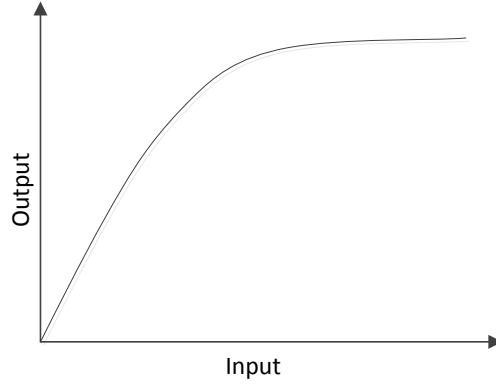


Figure 2.5: Typical AM/AM characteristic of a PA

### 2.1.1 Baseband Modeling

For a band limited RF simulation, illustrated in Fig. 2.6(a), the highest signal frequency is the sum of center frequency of the transmitter  $f_0$  and the highest baseband frequency  $B$ , where  $f_0 \gg B$ . According to the Nyquist theorem the sampling frequency must be

$$f_s = 2 \cdot f_{max} \quad (2.2)$$

to guarantee an aliasing free calculation. Such a high sampling frequency leads to an inefficient

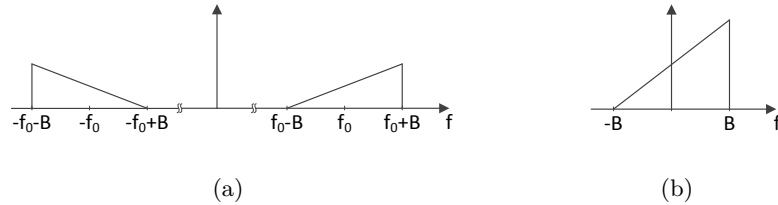


Figure 2.6: Frequency spectrum of RF- and Baseband model: (a) RF (b) Baseband

simulation as the frequency range  $0 < f < f_0 - B$  is unused. A more effective way is to shift the frequency range to the baseband as no relevant data is in  $f_0$ . The new frequency range  $-B < f < B$  requires only  $f_s = 2 \cdot B$ . In time domain the signal in RF band  $x(t)$  is represented by [9]

$$x(t) = \text{Re}\{A(t) \cdot e^{j2\pi f_0 t + \Phi(t)}\} = A(t) \cdot \cos(2\pi f_0 t + \Phi(t)) \quad (2.3)$$

where  $A(t)$  is the amplitude and  $\Phi(t)$  the phase of the signal. By changing the amplitude and the phase to real- and imaginary, the equation can be rewritten as

$$x(t) = \tilde{x}_r(t) \cdot \cos(2\pi f_0 t) - \tilde{x}_i(t) \cdot \sin(2\pi f_0 t) \quad (2.4)$$

where the signal  $\tilde{x}(t)$  is the original complex baseband signal

$$\tilde{x} = \tilde{x}_r + j\tilde{x}_i \quad (2.5)$$

modulated with the carrier frequency  $f_0$ . As seen a real valued signal in RF band can be transformed to a complex valued baseband signal.

A spectrum of a RF signal is always symmetric around 0 Hz. If this spectrum is shifted from RF to the baseband, it is not necessarily symmetric any more.

**Modeling of a Band-pass System** A band-pass system in RF can also be shifted to baseband. The simplest case would be a linear time-invariant (LTI) filter  $h(t)$  with the corresponding transfer function  $H(f)$  and a narrowband input signal  $X(f)$  [10]. The output can be described by

$$Y(f) = X(f) \cdot H(f). \quad (2.6)$$

For a baseband representation the filter must be shifted from the positive frequency domain to the baseband. Therefore, the system can be

$$\mathring{H}(f) = 2H(f)u(f) \quad (2.7)$$

where  $\mathring{H}(f)$  represents the analytic equivalent of  $H(f)$  and  $u(f)$  is the step function

$$u(f) = \begin{cases} 1 & \text{for } f \geq 0 \\ 0 & \text{otherwise.} \end{cases} \quad (2.8)$$

The analytical output can be calculated using (2.7) to

$$\begin{aligned} \mathring{Y}(f) &= X(f)\mathring{H}(f) \\ &= 2X(f)H(f)u(f) \\ &= \mathring{X}(f)H(f). \end{aligned} \quad (2.9)$$

Since there are no negative frequency components in  $\mathring{X}(f)$ ,  $H(f)$  can be extended to  $H(f)u(f)$ . Hence, (2.9) and (2.7) can be combined to

$$\mathring{Y}(f) = \frac{1}{2}\mathring{X}(f)\mathring{H}(f) \quad (2.10)$$

which can also be written in time domain [10]

$$\mathring{y}(t) = \frac{1}{2} \int_{-\infty}^{\infty} \mathring{h}(\tau)\mathring{x}(t-\tau)dt. \quad (2.11)$$

The analytical signal and the filter can be also expressed by their complex envelopes [10]

$$\mathring{x}(t) = \tilde{x}(t)e^{j2\pi f_0 t} \quad (2.12)$$

which show with (2.11) that

$$\begin{aligned}
 \hat{y}(t) &= \frac{1}{2} \int_{-\infty}^{\infty} \tilde{h}(\tau) e^{j2\pi f_0 \tau} \tilde{x}(t - \tau) e^{j2\pi f_0 (t - \tau)} dt \\
 &= \frac{1}{2} e^{j2\pi f_0 t} \int_{-\infty}^{\infty} \tilde{h}(\tau) \tilde{x}(t - \tau) dt \\
 &= \tilde{y}(t) e^{j2\pi f_0 t}
 \end{aligned} \tag{2.13}$$

and therefore the analytic output  $\hat{y}$  is a complex baseband signal which is centered around  $f_0$ . The baseband equivalent  $h_{BB}(t)$  of the filter  $h(t)$  is

$$h_{BB}(t) = \frac{1}{2} \tilde{h}(t). \tag{2.14}$$

In the case of a nonlinear system the harmonics around  $0, f_0, 2f_0, \dots$  which are produced by the nonlinearity have to be taken into account. Fig. 2.7 illustrates the effect of nonlinear

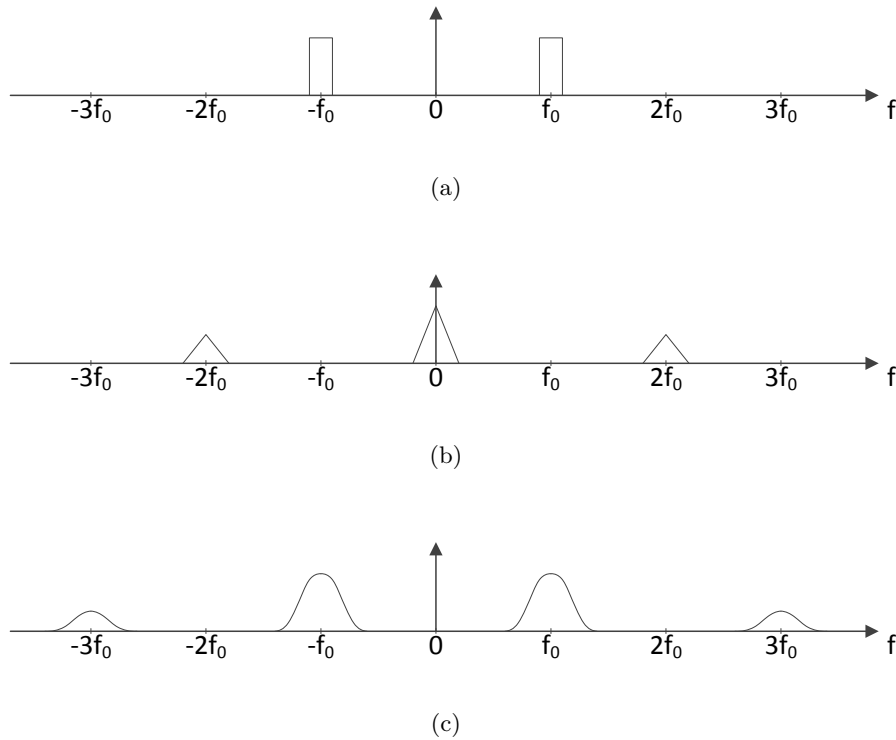


Figure 2.7: Frequency spectrum of a simple nonlinearity: (a)  $\mathcal{F}\{x(t)\}$  (b)  $\mathcal{F}\{x^2(t)\}, \mathcal{F}\{x^3(t)\}$ .

distortion to a rectangular input signal spectrum. It can be seen that even- and odd order distortions appear in different multiples of the carrier frequency. The frequency band can now be divided into zones (Fig. 2.8) where Zone 0 is the baseband and zone 1 the RF. Distortions of odd order only appear in odd zones and distortions of even order appear only in even zones. If the system is band-limited like the transmitter, the band limitation eliminates all zones except zone 1. Therefore, only distortions of odd order can appear on the output and even order

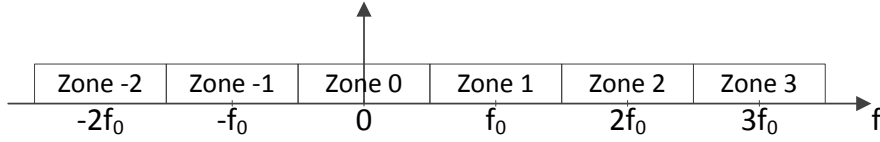


Figure 2.8: Zones in the frequency band.

distortions can be neglected. Using the derivation in [10] a nonlinear power series [11]

$$y(t) = \sum_{k=1}^K b_k x^k(t) \tag{2.15}$$

which in zone 1 can be transferred to the baseband form

$$\tilde{y}(t) = \sum_{\substack{k=1 \\ k \text{ odd}}}^K \tilde{b}_k \tilde{x}(t) |\tilde{x}|^{k-1} \tag{2.16}$$

where

$$\tilde{b}_k = \frac{1}{2^{k-1}} \binom{k}{\frac{k-1}{2}} b_k. \tag{2.17}$$

As shown in this section the transmitter can be fully described using an equivalent baseband model of the RF components. Therefore, all further elaboration will be done based on the equivalent baseband model.

### 2.1.2 Transmitter Analysis

To identify the transmitter, the output signal of the PA has to be compared with the input signal. Therefore, the amplified signal must be attenuated and converted to a digital signal. The identification can learn the behavior of the transmitter using algorithms elaborated in Section 3.2 and compensate the nonlinearities by creating a DPD which is placed in the transmitter path. The complete baseband transmitter using identification and DPD is illustrated in Fig. 2.9.

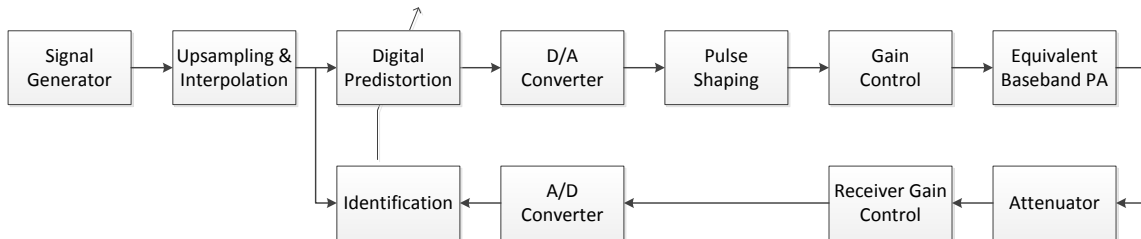


Figure 2.9: Baseband model of a transmitter using identification and DPD

## 2.2 Modeling the Power Amplifier

Nonlinearities of PAs can be either modeled physically or empirically [12]. The physical model means a circuit-level simulation, which requires some knowledge about how the PA is build. This method can produce a model which high accuracy at the expense of high computational complexity. Further on the resulting model is not flexible and can only be applied for this special PA. The second approach is to see the PA as black box [13] where the input/output (I/O) behavior can be observed. In this modeling approach there is no knowledge of the system required, but can be helpful to find the appropriate model. The models used for behavior modeling are elaborated in this section.

### 2.2.1 Volterra Series

A LTI System can be fully defined as [14, 15]

$$y[n] = \sum_{m=-\infty}^{\infty} h[m]x[n-m] \quad (2.18)$$

where  $h[m]$  represent the impulse response which needs to be

$$h[m] = 0 \text{ for } m < 0 \quad (2.19)$$

to be causal. Therefore, the sum in (2.18) can be limited to  $m \geq 0$ . The length of  $h[m]$  can be seen as the memory depth  $M$ . By setting the memory of the system to zero and extending the characteristic of the system to be nonlinear, the system could be represented by

$$y[n] = \sum_{p=0}^{\infty} c_p x^p[n]. \quad (2.20)$$

The combination of (2.18) and (2.20) leads to the general form of the Volterra series

$$\begin{aligned} y[n] = & h_0 + \sum_{m_1=0}^M h_1[m_1]x[n-m_1] \\ & + \sum_{m_1=0}^M \sum_{m_2=0}^M h_2[m_1, m_2]x[n-m_1]x[n-m_2] \\ & + \sum_{m_1=0}^M \sum_{m_2=0}^M \sum_{m_3=0}^M h_3[m_1, m_2, m_3]x[n-m_1]x[n-m_2]x[n-m_3] \\ & \vdots \\ & + \sum_{m_1=0}^M \cdots \sum_{m_p=0}^M h_p[m_1, \dots, m_p]x[n-m_1] \cdots x[n-m_p] \\ & + \cdots \end{aligned} \quad (2.21)$$

which can represent nonlinear time-invariant systems. The parameter of Volterra series  $h_p[m_1, \dots, m_p]$  are called Volterra kernels and are linear, even though the whole system behavior is nonlinear. Another way of expressing the Volterra series is using the Volterra operator

$$\underline{\mathbf{H}}_p[x[n]] = \sum_{m_1=0}^M \cdots \sum_{m_p=0}^M h_p[m_1, \dots, m_p] x[n - m_1] \cdots x[n - m_p] \quad (2.22)$$

instead of the Volterra kernels. The use of the Volterra operator rearranges (2.21) to

$$y[n] = h_0 + \sum_{p=1}^P \sum_{m_1=0}^M \sum_{m_2=0}^M \cdots \sum_{m_p=0}^M h_p[m_1, m_2, \dots, m_p] \prod_{k=1}^p x[n - m_k], \quad (2.23)$$

where P represents the order of the nonlinearity. The structure of the Volterra series using Volterra kernels is illustrated in Fig. 2.10. The Volterra series can be shifted from passband

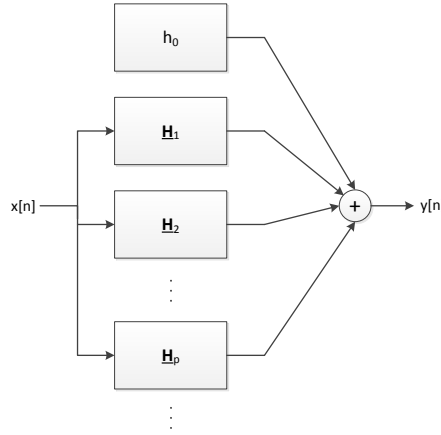


Figure 2.10: Schematic representation of a volterra series.

to baseband using the knowledge of Section 2.1.1. Therefore, (2.23) can be rewritten to the complex baseband form [11, 16]

$$\begin{aligned} \tilde{y}[n] = & \tilde{h}_0 + \sum_{p=1}^P \sum_{m_1=0}^M \sum_{m_2=0}^M \cdots \sum_{m_{\lfloor \frac{p+1}{2} \rfloor} = m}^M \sum_{m_{\lfloor \frac{p-1}{2} \rfloor} = m}^M \cdots \sum_{m_p = m_{p-1}}^M \tilde{h}_p[m_1, m_2, \dots, m_p] \\ & \times \prod_{i=1}^{\lfloor \frac{p+1}{2} \rfloor} \tilde{x}[n - m_i] \prod_{k=\lfloor \frac{p+3}{2} \rfloor}^p \tilde{x}^*[n - m_k]. \end{aligned} \quad (2.24)$$

To visualize the Volterra kernels, a simple example using  $P = 2$  and  $M = 4$  is illustrated as

$$\tilde{h}_1[m_1] = \begin{bmatrix} \tilde{h}_1[0] \\ \tilde{h}_1[1] \\ \tilde{h}_1[2] \\ \tilde{h}_1[3] \end{bmatrix}, \quad \tilde{h}_2[m_1, m_2] = \begin{bmatrix} \tilde{h}_2[0, 0] & \tilde{h}_2[0, 1] & \tilde{h}_2[0, 2] & \tilde{h}_2[0, 3] \\ \tilde{h}_2[1, 0] & \tilde{h}_2[1, 1] & \tilde{h}_2[1, 2] & \tilde{h}_2[1, 3] \\ \tilde{h}_2[2, 0] & \tilde{h}_2[2, 1] & \tilde{h}_2[2, 2] & \tilde{h}_2[2, 3] \\ \tilde{h}_2[3, 0] & \tilde{h}_2[3, 1] & \tilde{h}_2[3, 2] & \tilde{h}_2[3, 3] \end{bmatrix} \quad (2.25)$$

where  $\tilde{h}_1$  is the first-, and  $\tilde{h}_2$  the second order Volterra kernel.

**Summary** The Volterra series is a powerful approach to model any kind of time-invariant nonlinearities. The drawback of the flexibility is the huge amount of parameters which have to be identified. Every kernel of order  $p$  has  $M^p$  parameter. Due to symmetry [17] the number of parameters per kernel can be reduced to

$$N_p = \binom{M+p}{p} \quad (2.26)$$

independent parameters for the RF band and [18]

$$\tilde{N}_p = \binom{M + \lfloor \frac{p-1}{2} \rfloor}{\lfloor \frac{p-1}{2} \rfloor} \binom{M + \lceil \frac{p-1}{2} \rceil}{\lceil \frac{p-1}{2} \rceil} \quad (2.27)$$

for the baseband model. Despite the reduction the total amount of parameter  $N = \sum_{p=1}^P N_p$  and therefore also the computational complexity in a Volterra series is growing rapidly by increasing the order of the nonlinearity. To reduce the number of parameter different approaches are made to simplify the full Volterra series to reduced- or pruned Volterra series models.

### 2.2.2 Memoryless Model

The easiest simplification of the Volterra series is the use without memory. This model is an easy approach to allow modeling only the effects of the nonlinearity and is therefore often used in combination with linear filter like in Wiener- or Hammerstein models [11, 13]. The memoryless model can be expressed using a complex power series [11]

$$\tilde{y}_{MLP}[n] = \sum_{\substack{p=1 \\ p \text{ odd}}}^P \tilde{a}_p \tilde{x}[n] |\tilde{x}[n]|^{p-1} \quad (2.28)$$

where  $a_p$  are the complex valued coefficients of a polynomial. Therefore, this model also is called memoryless polynomial (MLP). The realization of a MLP using a Volterra series changes the kernels to

$$\tilde{h}_p[m_1, m_2, \dots, m_p] = \begin{cases} \tilde{a}_p & \text{if } m_1 = m_2 = \dots = m_p = 0 \\ 0 & \text{otherwise,} \end{cases} \quad (2.29)$$

which would simplify the example from (2.25) to

$$\tilde{h}_1[m_1] = \begin{bmatrix} \tilde{a}_1 \\ 0 \\ 0 \\ 0 \end{bmatrix}, \quad \tilde{h}_2[m_1, m_2] = \begin{bmatrix} \tilde{a}_2 & 0 & 0 & 0 \\ 0 & 0 & 0 & 0 \\ 0 & 0 & 0 & 0 \\ 0 & 0 & 0 & 0 \end{bmatrix}. \quad (2.30)$$

**Summary** The MLP is a good model to describe nonlinearities without any other effects. Due to the simplicity the number of independent parameter is only  $N = P$ . This model is often used when the nonlinearity can be split into a nonlinear part and an additional linear filter.

### 2.2.3 Memory Polynomial

Another pruned Volterra model which already includes memory is the memory polynomial (MP). This model is often used for describing the nonlinear effects of PAs [11,12]. The I/O relationship of a MP is given by

$$\tilde{y}_{MP}[n] = \sum_{\substack{p=1 \\ p \text{ odd}}}^P \sum_{m=0}^M \tilde{h}_p[m] \tilde{x}[n-m] |\tilde{x}[n-m]|^{p-1}. \quad (2.31)$$

The comparison with a Volterra series shows

$$\tilde{h}_p[m_1, m_2, \dots, m_n] = \begin{cases} \tilde{h}_{p,m} & \text{if } m_1 = m_2 = \dots = m_n \\ 0 & \text{otherwise} \end{cases} \quad (2.32)$$

and can be illustrated using example (2.25)

$$\tilde{h}_1[m_1] = \begin{bmatrix} \tilde{h}_1[0] \\ \tilde{h}_1[1] \\ \tilde{h}_1[2] \\ \tilde{h}_1[3] \end{bmatrix}, \quad \tilde{h}_2[m_1, m_2] = \begin{bmatrix} \tilde{h}_2[0,0] & 0 & 0 & 0 \\ 0 & \tilde{h}_2[1,1] & 0 & 0 \\ 0 & 0 & \tilde{h}_2[2,2] & 0 \\ 0 & 0 & 0 & \tilde{h}_2[3,3] \end{bmatrix}. \quad (2.33)$$

**Summary** The MP is a popular way of describing the behavior of wideband PAs which are affected by memory. The number of independent coefficients are  $N = P \cdot (M + 1)$ .

### 2.2.4 Quasi-memoryless Model

A system can be considered as Quasi-memoryless (QMM) if the memory is small enough that the distortions only depend on the current input signal [19]. Such systems can be described by the AM/AM conversation (AM/AM), and AM/PM conversation (AM/PM) which are elaborated in Section 4.1.1 on page 28. The measurement of the characteristics can be easily performed with a single tone sweep using a vector network analyzer (VNA). The I/O representation of the QMM is

$$\tilde{y}_{QMM}[n] = f_A(|\tilde{x}[n]|) \cdot e^{j \cdot \angle \tilde{x}[n] \cdot f_P(|\tilde{x}[n]|)} \quad (2.34)$$

where  $f_A(|\tilde{x}[n]|)$  is the AM/AM and  $f_P(|\tilde{x}[n]|)$  is the AM/PM conversation. For the realization of a QMM, the AM/AM and AM/PM can be implemented using polynomials or Look-up tables (LUTs). The LUT is often used in implementation on hardware due to their simplicity. On runtime the LUT does not have to perform any complex calculations but find the right entry for

the given input. The limiting parameter of the LUT is the numbers of entries as it is determined by the physical memory which is used in the hardware.

**Summary** The popularity of the QMM is based on the simplicity of measuring the AM/AM and AM/PM characteristic of PAs and the simple implementation. Due to the small memory, which can be represented by the QMM it leads to good results for narrowband systems but does not work for wideband systems.



## 3

## Calibration Methods

## 3.1 Preprocessing

The preprocessing is the first step of the identification with the goal of simplifying the later identification task by compensating the most significant linear differences between the I/O signals of the transmitter. The default used block is illustrated in Fig. 3.1. Every step of the preprocessing is separated to estimation and correction block to allow switching between different methods.

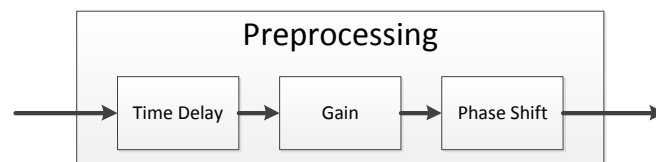


Figure 3.1: Preprocessing block.

**Time Delay** Due to the latency of the transmitter, the output signal is delayed compared to the input signal (see Fig. 3.2). By compensating this delay during the preprocessing, the memory of the identified model can be reduced. The estimation of this delay is performed by a two stepped algorithm that first estimates the integer delay and then the fractional delay. The integer delay estimation is achieved using a cross-correlation of the in- and the output signal. A minimization of the cross-correlation, filtered by a fractionally shifted sinc is used for the calculation of the fractional delay. After this estimation the algorithm shifts the time domain signal by filtering the signal with a fractionally delayed sinc for the fractional delay and by deleting the not needed samples for the integer delay. This operation does not introduce any

additional phase shifts between in-phase and the quadrature component and does not change the gain.

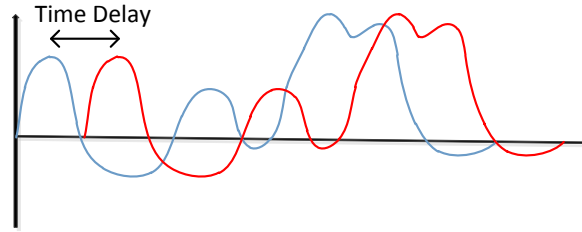


Figure 3.2: Illustration of a time delay.

**Gain** The gain correction normalizes the output signal so that the gain factor between the input and the normalized output is around 1. For the estimation of the gain factor different algorithms can be used. These algorithms define the linear range of the PA output signal and the gain. Fig. 3.3 illustrates the gain correction for the maximum linearity algorithm which use the gain factor

$$g_{max_{lin}} = \frac{|x_i|}{|y_i|} \Big|_{|x_i|=\max(|\mathbf{X}|)} \tag{3.1}$$

and the maximum gain algorithm which use the DC gain of the PA. The advantage of maximum linearity is the linearity of the whole signal range which can be realized by reducing the gain of the entire transmitter. The advantage of the maximum gain estimation is that the slope of the transmitter is linear up to a saturation point. Input amplitudes above this saturation point cannot be amplified anymore and therefore stay constant on the output. To identify the PA the maximum linearity estimation can be used to find the perfect inverse. As the aim of the transmitter is not to reduce the DC gain of the PA, the perfect inverse must be scaled to adjust the gain.

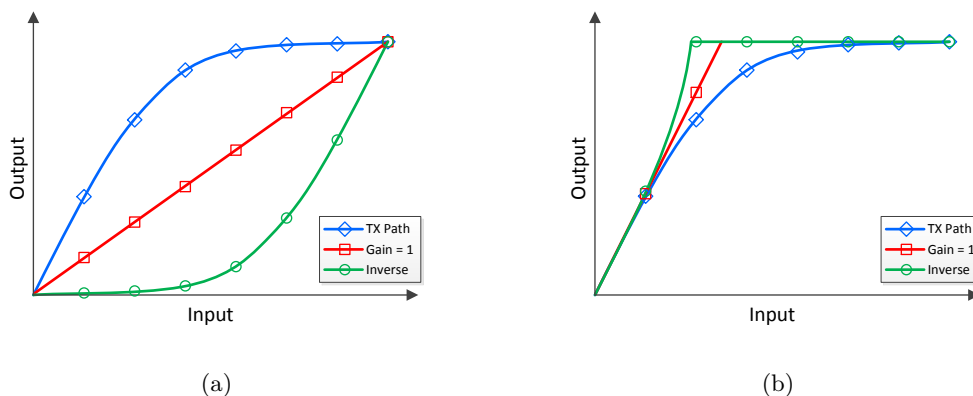


Figure 3.3: AM/AM characteristic with different gain-factors: (a) Maximum Linearity Estimation (b) Maximum Gain Estimation

**Phase shift** The phase correction changes the phase of the complex baseband output signals in order to be aligned with the phase of the input signal. This operation is realized by averaging the phase shifts of all symbols namely

$$\hat{\phi}_{avg} = \angle(\mathbf{X}^H \cdot \mathbf{Y}) \quad (3.2)$$

and is equivalent to a rotation of the whole constellation diagram which is illustrated in Fig. 3.4.

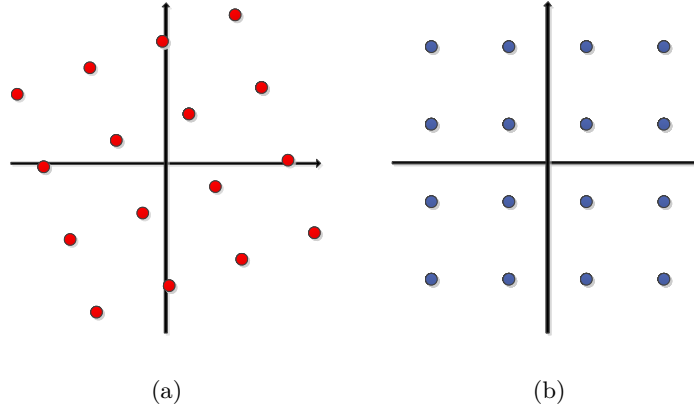


Figure 3.4: Compensation of a phase shift: (a) before compensation, (b) after compensation.

## 3.2 Used Identification Procedure

The aim of a transmitter is to amplify the input signal with a constant gain factor. As shown in Section 2.1 the PA does not have a constant gain in the whole input range. Further on there are band limiting filters in the transmitter which lead to nonlinear distortions. To compensate these nonlinear distortions the exact system behavior has to be known. A common way of identifying the model parameter is to approximate them using approximation algorithms like least squares (LS) or least mean squares (LMS) [20, 21]. For a good identification it is also important to know how the unknown system looks and find a good behavioral model which represents the nonlinearities as described in Section 2.2. The algorithm used to find the model parameters is specified in this Section.

**Least Squares Approximation** The transmitter is assumed to be an unknown system  $\mathbf{H}$  which is illustrated in Fig. 3.5. The ideal output of this system should be an amplified, time delayed and phase shifted version of the input signal  $x[n]$  which is represented as the desired output signal  $d[n]$ . The error between the output and the desired output

$$e[n] = y[n] - d[n] \quad (3.3)$$

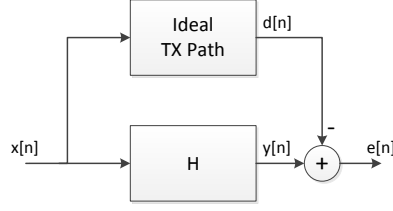


Figure 3.5: Basic structure of a identification process.

is used to create the cost function  $J_k$  for the LS approximation which is defined as [20]

$$J_k = \sum_{n=n_0}^k |e[n]|^2 = \sum_{n=n_0}^k |y[n] - d[n]|^2. \quad (3.4)$$

The output  $y[n]$  can be calculated using [21]

$$y[n] = \sum_{l=0}^{M-1} x[n-l]h_l \quad (3.5)$$

where  $x[n]$  is the input signal and  $w_l$  are the coefficients of the unknown system. This equation can be written in matrix form

$$\mathbf{y} = \mathbf{X}\mathbf{h} \quad (3.6)$$

where  $\mathbf{X}$  is the matrix which holds input vectors for all the time instances. Similar to this the desired output can be calculated as

$$\mathbf{d} = \mathbf{X}\mathbf{w} \quad (3.7)$$

where  $\mathbf{w}$  are the parameter of the ideal transmitter. By minimizing the cost function (3.4) the outputs should become  $\mathbf{y} \approx \mathbf{d}$  and the unknown parameter can be estimated. In MATLAB this operation can be performed using the backslash operator [22]  $\mathbf{h} = \mathbf{x} \setminus \mathbf{d}$ . To apply this method on a Volterra series (2.23) the nonlinear problem have to be transferred to a linear matrix form

$$y[n] = \mathbf{x}^T[n]\mathbf{h}. \quad (3.8)$$

Therefore the vectors can be created as [23]

$$\mathbf{x}[n] = [1, x[n], x[n-1], \dots, x[n-M], x^2[n], x[n]x[n-1], \dots, x^2[n-M], x^3[n], \dots]^T \quad (3.9)$$

and

$$\mathbf{h} = [h_0, h_1[0], h_1[1], \dots, h_1[M], h_2[0,0], h_2[0,1], \dots, h_2[M,M], h_3[0,0,0], \dots]^T. \quad (3.10)$$

The output vector  $\mathbf{y}$  can be calculated using (3.8), (3.9) and (3.10) to

$$\mathbf{y} = \begin{bmatrix} \mathbf{x}^T[0] \\ \mathbf{x}^T[1] \\ \vdots \end{bmatrix} \mathbf{h}. \quad (3.11)$$

Due to the low complexity and the good estimation performance, the LS estimation is further used for the offline identifications. For a real-time implementation a more sophisticated estimation method must be used.



## 4

## Calibration Performance

In this chapter the simulation and evaluation is performed and discussed. To determine the quality of the results all the relevant measurement methods are introduced first. Next the model of the PA and the transmitter are evaluated to find the best possible performance which can be achieved using the given models. In the end the transmitter and the DPD will be identified using LS identification and the performance is evaluated for the desired output power levels of 17 dBm and 19 dBm.

For the input signal of the simulations a pseudo-OFDM signal is chosen to allow EVM measurements. The detailed definition of this signal is shown in Tab. 4.1. According to this configuration the EVM must be below -25 dB as specified in Tab. 1.4.

Power	Modulation	Code Rate	Rate	PAPR	Symbols
-10 dBm	64-QAM	$3/4$	200 Mbit/s	$\approx 10$ dB	100

Table 4.1: Definition of the pseudo-OFDM signal.

## 4.1 Quality of the Measurements

This section introduces all tools which are required to analyze the performance of the transmitter and the identification. The first part describes methods how characteristics can be illustrated in plots and the second part defines figures of merits (FOMs). To describe the methods the vector  $\mathbf{x}$  is used as input signal and  $\mathbf{y}$  is the output signal of the transmitter.

### 4.1.1 Plots

**Power Spectral Density** The PSD is the frequency representation of the signal which gives the distribution of the power in frequency domain. A simple way of calculating the frequency response of a signal is using a Fourier transformation. In order to be able to measure data directly from the PSD effects like spectral leakage and the scaling of the spectrum have to be taken care of. To define the resolution of the fast Fourier transformation (FFT) a long signal must be cut to smaller pieces which is done in a spectrum analyzer using a resolution bandwidth (RBW) filter. In order to calculate the PSD with respect to one Hz and not the input bandwidth, the signal has to be scaled [24]. Spectral leakage occurs when the signal is not periodic within the FFT length and produces discontinuities at the beginning and the end of the signal section. This effect can be avoided using a window function like Hann, Hamming, etc. [25]. The multiplication of the window and the signal in time domain change the power in the signal, wherefore another scaling factor [24] have to be taken into account. For an accurate measurement the signal has to be normalized with respect to the impedance  $R$  which is used in the hardware. Another approach of implementing the PSD using MATLAB is the `pwelch` function. This function cuts the input signal to smaller segments and averages the segments for a robust estimation of the PSD.

**AM/AM and AM/PM** A transmitter can be also evaluated by the AM/AM conversation (AM/AM) and the AM/PM conversation (AM/PM). These plots illustrate the direct relationship between the amplitude and the phase of the I/O signals. The two functions can be written as

$$f_A(|\mathbf{x}|) = |\mathbf{y}| \quad (4.1)$$

$$f_P(|\mathbf{x}|) = \angle \mathbf{y} - \angle \mathbf{x} \quad (4.2)$$

where  $f_A(|\mathbf{x}|)$  is the function of the AM/AM and  $f_P(|\mathbf{x}|)$  the function of the AM/PM. As this plot is in time domain it is important to have no time delay between the I/O signals.

### 4.1.2 Figures of Merit

**Signal Power** The signal power describes the root mean square (RMS) power level of the signal in dBm and is

$$P_x = 10 \log \left( \frac{U_{RMS}(\mathbf{x})}{\frac{R}{10^{-3}}} \right) \quad (4.3)$$

where  $U_{RMS}(\mathbf{x}) = \sqrt{\frac{1}{N} \sum \mathbf{x}^2}$ ,  $N$  is the length of the signal and  $R$  the impedance of the hardware.

**Peak to average power ratio** The peak-to-average power ratio (PAPR) gives the ratio of the peak power of the signal to the RMS power in dB and is defined as

$$PAPR = 20 \log \left( \frac{\max |\mathbf{x}|}{U_{RMS}(\mathbf{x})} \right). \quad (4.4)$$

**Signal to Noise Ratio** The signal to noise ratio (SNR) can be calculated as

$$SNR_{dB} = 10 \cdot \log \left( \frac{\sum \mathbf{x}^2}{\sum |\mathbf{y} - \mathbf{x}|^2} \right) \quad (4.5)$$

and is used to compare the signals  $\mathbf{x}$  and  $\mathbf{y}$ . If the signals does match perfectly ( $\mathbf{x} = \mathbf{y}$ ) the SNR is infinity. The smaller the SNR, the more difference is between the signals.

**Error Vector Magnitude** The error vector is defined as the distance in the constellation diagram between the original OFDM symbol and the received demodulated symbol which is illustrated in Fig. 4.1. The error vector magnitude (EVM) is calculated by averaging the error vectors [12]

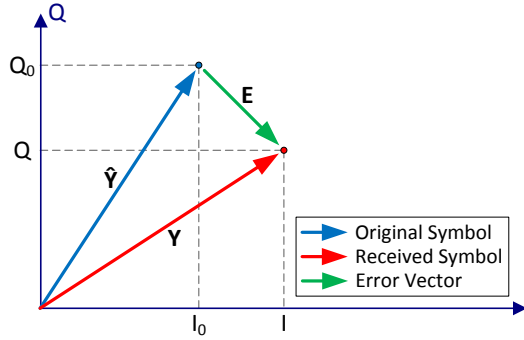


Figure 4.1: Error vector of an OFDM symbol.

$$EVM = \sqrt{\frac{\sum_n |y[n] - \hat{y}[n]|^2}{\sum_n |y[n]|^2}} \quad (4.6)$$

where  $y[n]$  is the measured output of the system and  $\hat{y}[n]$  the output of the model.

**Adjacent Channel Power Ratio** The adjacent channel power ratio (ACPR) gives the out-of-band power of the signal with respect to the in-band power and is used to evaluate the out-of-band behavior of the signal. It can be calculated by [11]

$$ACPR = \frac{\int_{adj} |Y(f)|^2 df}{\int_{ch} |Y(f)|^2 df} \quad (4.7)$$

where  $Y(f)$  is the Fourier transform of the signal  $\mathbf{y}$ . Fig. 4.2 illustrate the location of the main and the adjacent channels.

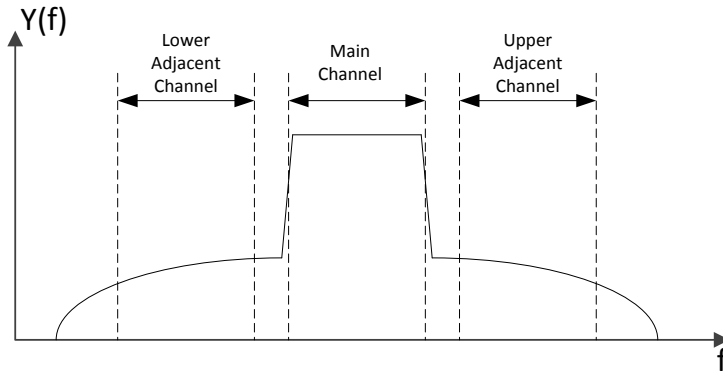


Figure 4.2: Main- and Adjacent channel.

**Mask distance** The mask distance  $d$  is the distance of the out-of-band signal to the spectral mask which is defined in Section 1.4.2 on page 4. A positive  $d$  indicates that the signal power is below the mask whereas a negative  $d$  indicates a mask violation.

## 4.2 PA Model

The model used for the PA is stored in a QMM-LUT with 265 entries using spline interpolation which is created by an amplitude sweep measurement of a single tone on the RFIC. To get a good fit the measured data was firstly fitted using QMM polynomials where the order of the AM/AM polynomial is 7 and the AM/PM polynomial is 5. The fitted polynomials were converted to a LUT for further calculations because operations like inverting are simpler to perform on this model. The characteristic of the model is illustrated in Fig. 4.3 and the specifications of the measured characteristic are shown in Tab. 4.2. By using the maximal output voltage and

Small Signal Gain	30.76 dB
Maximal Output Voltage	5.16 V

Table 4.2: Specification of the QMM PA model.

a defined PAPR the output power of a perfectly linearized PA can be calculated by rewriting (4.4) to

$$U_{RMS}(\mathbf{y}) = \frac{\max |\mathbf{y}|}{10^{\frac{PAPR}{20}}} \quad (4.8)$$

and using (4.3). Tab. 4.3 shows the resulting output power for a varying PAPR. It can be seen that for the desired output power of 17 dBm the transmitter can be theoretically linearized.

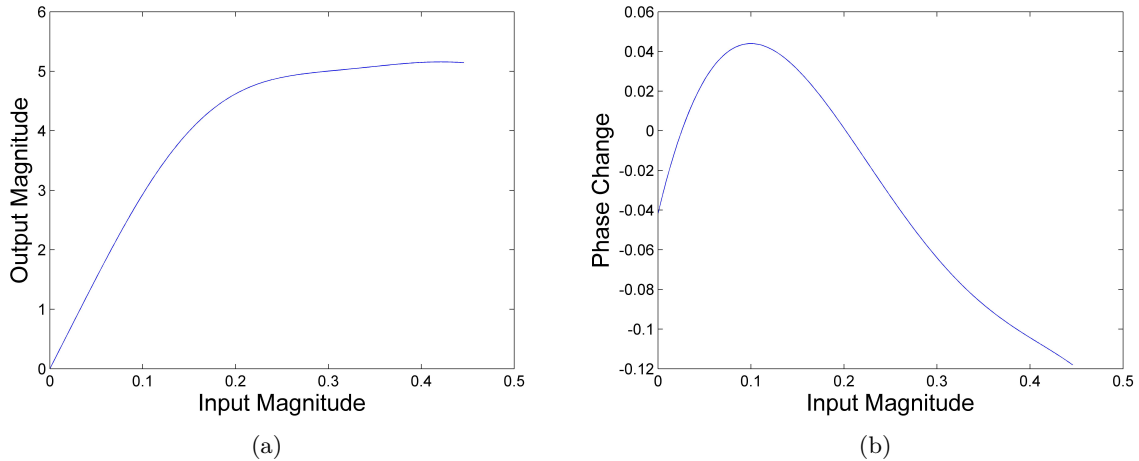


Figure 4.3: Characteristic of the PA model (a) AM/AM, (b) AM/PM.

For a higher output power the idealized PA must be used in saturation wherefore clipping does occur.

PAPR / dB	Power / dBm
10.0	17.26
10.5	16.76
11.0	16.26
11.5	15.76
12.0	15.26

Table 4.3: Maximal output power for defined PAPR.

## 4.3 Idealized Transmitter

In this section the idealized transmitter is simulated to find the best possible performance of the implemented MATLAB model. The system components are called idealized because they are modeled by knowing all the parameter which means no identification will be performed in this section. Therefore, the first step is to evaluate the performance without any predistortion. In the second step the inverse of the PA model is created to equalize the nonlinearities. To complete the transmitter the influence of the pulse shaping filter which introduces memory is taken into account in the third step. A practical implementation of the DPD using a LUT does only provide a limited amount of entries. Therefore, the last part in this section will evaluate the influence of different sizes of the LUT and interpolation methods.

### 4.3.1 Performance Evaluation

The first step is to evaluate the performance of the transmitter without DPD for different pre-gain levels. The structure used for the simulation is illustrated in Fig. 2.9 where no DPD and

receive power control is used to see the influence of different pre-gain levels. The results of this simulation are concluded in Tab. 4.4. It can be seen that by increasing the pre-gain, the total

Pre Gain /dB	Output Power /dBm	EVM /dB	ACPR /dB	d /dB
-11	8.46	-40.01	-39.03	10.92
-9	10.45	-39.11	-38.83	10.85
-7	12.44	-38.33	-38.62	10.80
-5	14.40	-37.19	-38.28	10.71
-3	<i>16.32</i>	<i>-34.67</i>	<i>-37.37</i>	<i>10.42</i>
-1	<i>18.18</i>	<i>-30.62</i>	<i>-35.26</i>	<i>9.49</i>
1	<i>19.93</i>	<i>-26.03</i>	<i>-31.98</i>	<i>6.96</i>
3	21.52	-21.66	-28.34	3.19
5	22.90	-18.81	-25.00	-0.71

Table 4.4: Simulation results of the transmitter (desired output power range in italic).

output power increases at the cost of EVM and ACPR. For the pre-gain of 5 the mask distance is negative which means that the spectral mask is violated. Further on it can be seen that the EVM for the pre-gain levels 3 dB and 5 dB are higher than the required -25 dB. The desired output power can be achieved using pre-gain levels from -3 to 1 dB. Fig. 4.4 illustrates the behavior of the output signal in frequency domain for two different pre-gain levels. Also here the mask violation can be seen in the figure with the higher pre-gain.

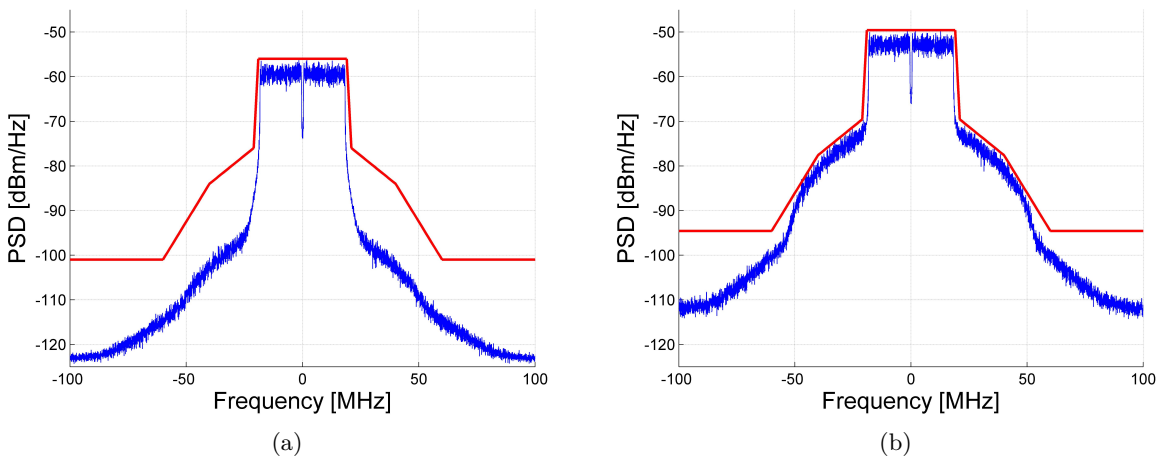


Figure 4.4: PSD of the transmitter without DPD and pre-gain of (a) -3 dB, (b) +5 dB.

To complete this analysis the effects in time domain have to be evaluated as well, which can be done using the AM/AM and the AM/PM. These plots are illustrated in Fig. 4.5. The nonlinear effect can be seen as the AM/AM is not linear anymore for the higher pre-gain levels. Another effect which can be seen is that the AM/AM and the AM/PM are not thin lines any more like in Fig. 4.3. This effect can either be caused by memory in the transmitter or by a timing misalignment of the I/O signals. As the I/O signals are synchronized by the pre-processing and the PA model is QMM this effect is caused by the memory of the pulse shaping filter. As elaborated in Section 2.1 the pulse shaping filter can be also moved in the system chain into

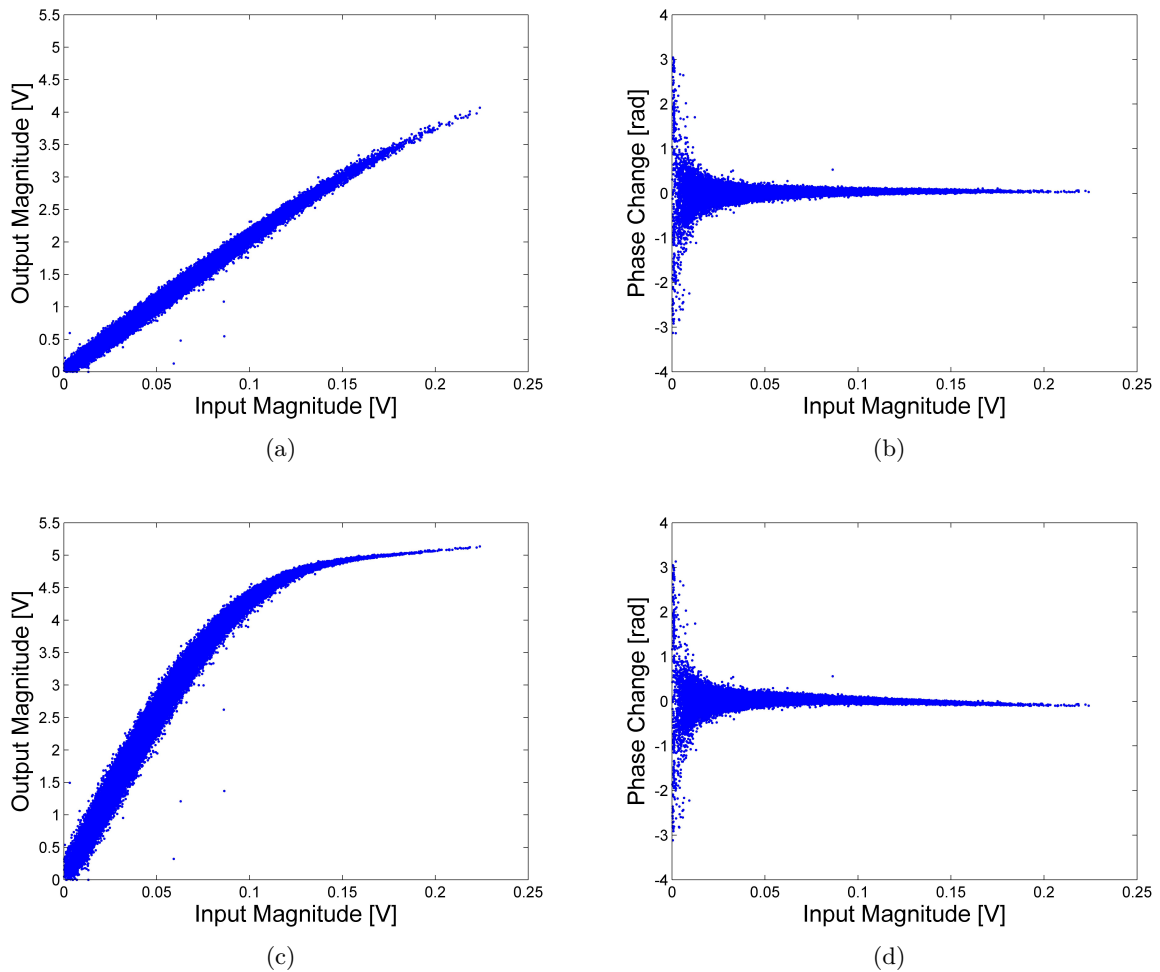


Figure 4.5: Evaluating influences of transmitter in time domain without DPD and pre-gain of (a) AM/AM: -3 dB, (b) AM/PM: -3 dB, (c) AM/AM: +5 dB, (d) AM/PM: +5 dB.

the signal generator if the DAC ensures not to violate the spectral requirements. Therefore the transmitter is simulated without the pulse shaping filter to proof that the other components of the transmitter are memoryless. The results are illustrated in Fig. 4.6 and in Tab. 4.5. It can be seen that the EVM and the ACPR decrease marginal as compared to the results from Tab. 4.4. The AM/AM and the AM/PM shows that there is no more memory effect in the transmitter path.

**Bounds of the simulation** To elaborate what is the best possible performance which can be achieved using the implemented model the transmitter is simulated without PA. The pre-gain does not effect this simulation as it is compensated in the receive path. The result of this simulation is shown in Tab. 4.6. To find the limiting parameter of the simulation the resolution of the DAC is increased to 16 bit. It can be seen that the higher resolution does decrease the EVM. Therefore, the limiting parameter is the resolution of the DAC which is defined with 10 Bit.

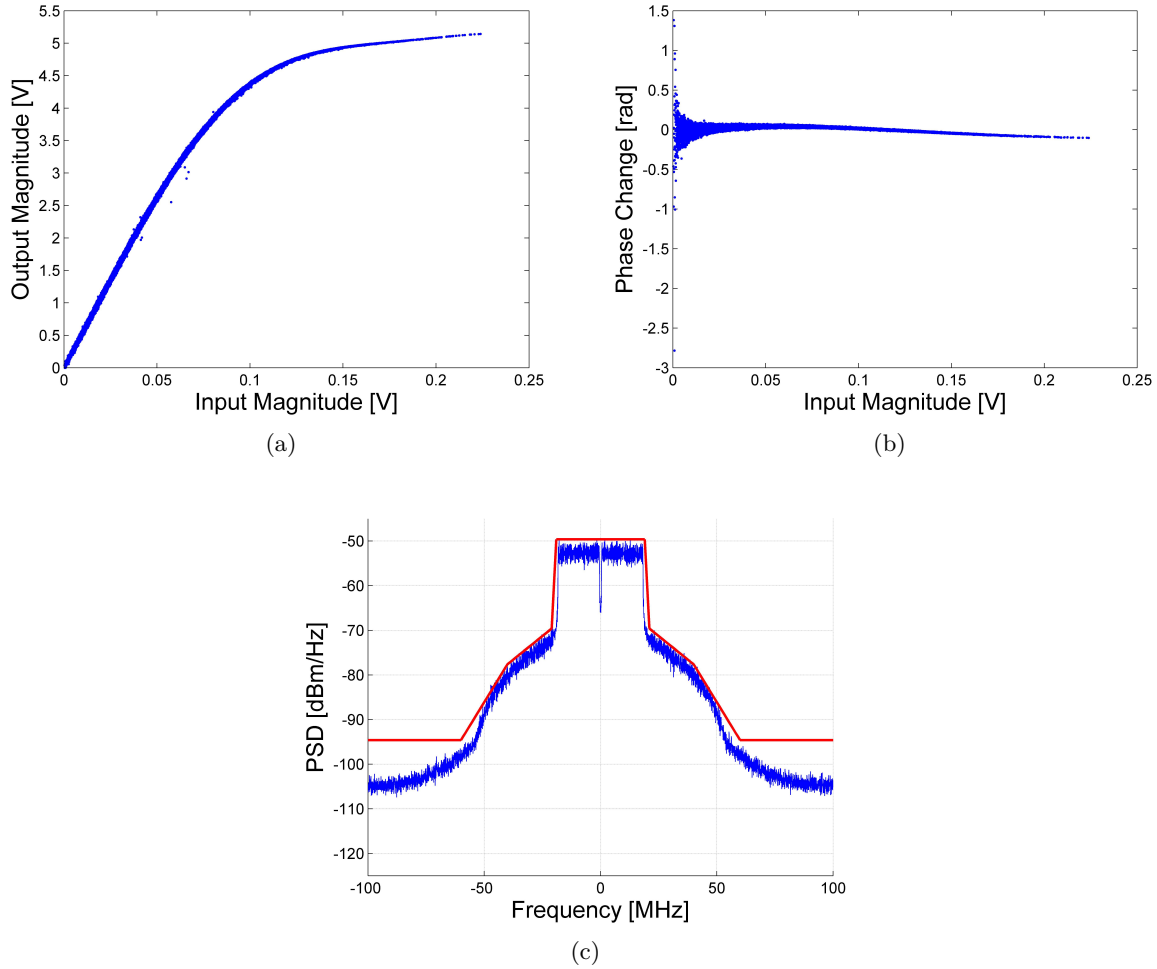


Figure 4.6: Transmitter without pulse shaping filter, DPD and a pre-gain of +5 dB (a) AM/AM, (b) AM/PM, (c) PSD.

Pre Gain /dB	Output Power /dBm	EVM /dB	ACPR /dB	d /dB
-11	8.66	-39.92	-36.79	7.99
-9	10.65	-39.05	-36.66	7.81
-7	12.64	-38.26	-36.52	7.60
-5	14.60	-37.03	-36.27	7.26
-3	16.52	-34.34	-35.58	6.87
-1	18.36	-30.20	-33.88	6.45
1	20.10	-25.62	-31.03	5.63
3	<i>21.68</i>	<i>-21.30</i>	<i>-27.68</i>	<i>2.40</i>
5	<i>23.04</i>	<i>-18.61</i>	<i>-24.50</i>	<i>-1.52</i>

Table 4.5: Simulation results of the transmitter without pulse shaping filter. (The region where 802.11n is violated is represented in italic.)

DAC Resolution /Bits	EVM /dB	ACPR /dB	d /dB
10	-52.49	-39.91	11.32
16	-85.45	-39.93	11.32

Table 4.6: Simulation of the transmitter without PA.

### 4.3.2 Ideal Inverse of the PA

The first goal is to perfectly compensate the nonlinearities of the PA by using all the knowledge of the system model to create a perfect inverse of the PA for the DPD. Therefore, the pulse shaping filter is assumed to be implemented within the signal generator and removed from the transmitter. The performance of this system will be evaluated and is used as reference for further simulations. In the second approach the pulse shaping filter is taken into account and the differences in performance are elaborated.

**Creating the DPD** For the creation of the ideal inverse of the PA a QMM-LUT with 256 entries and spline interpolation is used. The advantage of the LUT instead of a polynomial approach is that the characteristic can be directly measured using an amplitude sweep of a single tone without knowing the order of the nonlinearity. The concept how the amplitude predistortion works is illustrated in Fig. 4.7 where  $X$  is the input signal and  $Y_1$  the output signal of the PA. If the DPD is used before the PA, the output of the DPD is  $Y_{DPD}$  which is also the input of the PA  $X_{PA}$ .  $Y_2$  is therefore the output of the system where the DPD and the PA are used. The overall characteristic of the system using the DPD and the PA is illustrated as red line which is linear up to the maximal output of the PA. It can be seen that the  $Y_2$  equals the linear output for the input  $X$ . In the transmitter the DAC, which have a limited input range, is between the DPD and the PA. If the gain in the DPD is too high clipping occurs.

The DPD can be created by exchanging the input and the output of the original AM/AM. As the new input vector is no longer linear, an interpolation must be performed to find the inverse output of the desired linear input vector. For the inverse AM/PM the distortion of the amplitude has to be taken into account. Therefore, the original AM/PM must be interpolated using the inverse AM/AM characteristic as input to find the inverse AM/PM. The resulting characteristics are stored in a LUT. Fig. 4.8 illustrates the AM/AM and AM/PM of the PA without small signal gain and the resulting DPD. As the adjustment of the pre-gain change the used range of the PA, the range of the DPD have to be adjusted as well for every pre-gain level. This can be accomplished by adjusting the in- and output gain of the DPD which is illustrated in Fig. 4.9. Using this technique, the DPD have to be created ones for a pre-gain of 0 dB and the scaling is done afterwards.

**Transmitter without pulse shaping filter** The first simulation is performed without pulse shaping filter and different pre-gain levels to evaluate the performance of the DPD. The results of this simulation are shown in Tab. 4.7. It can be seen that for pre-gain levels below -3 dBm the EVM is the same as if the PA were removed from the transmitter, which is shown in Tab. 4.6. In this region the lower bound is limited by the quantization noise of the analog to digital converter (ADC). A higher pre-gain leads to hard clipping of the linearized transmitter which increases the EVM and decreases the mask distance. Due to this hard clipping the performance of the linearized transmitter is similar to the performance of the transmitter without DPD for pre-gain levels above 1 dB. The effect of clipping in the linearized transmitter is illustrated in Fig. 4.10 where the PSD and the AM/AM for the output signal of different pre-gain levels are illustrated. It can be seen that the simulation in (b) does have a higher output power, but also

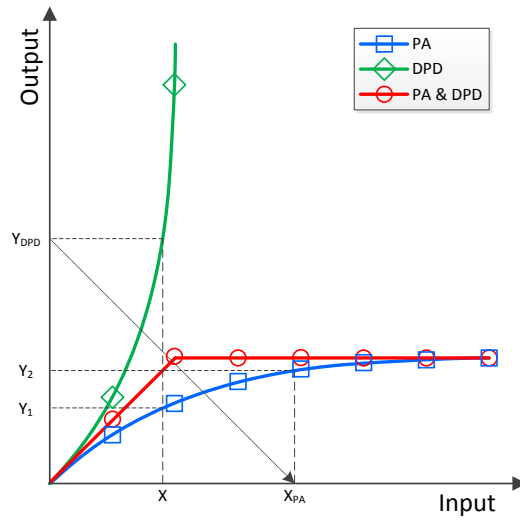


Figure 4.7: Principle amplitude distortion in DPD.

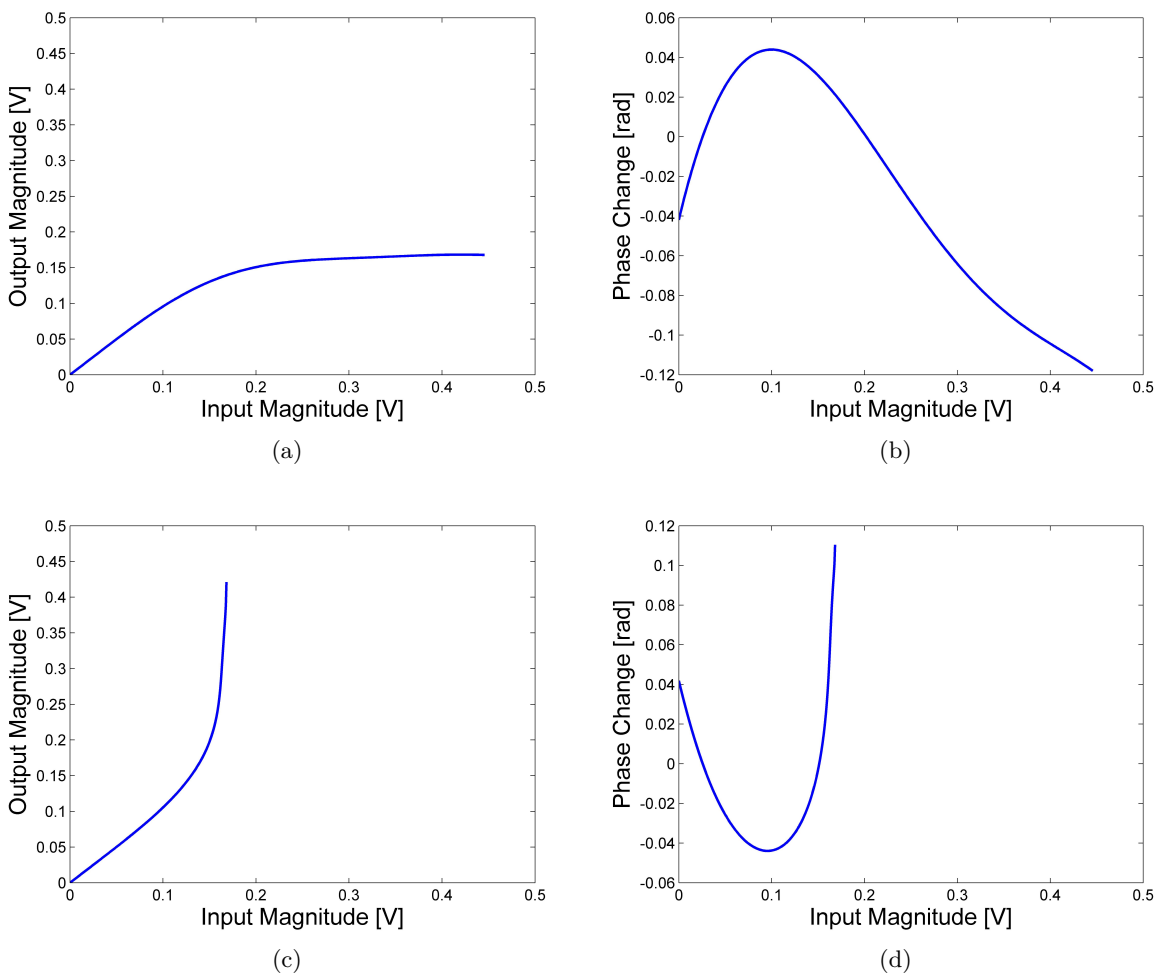


Figure 4.8: Amplitude- and Phase characteristic of the normalized PA and the DPD (a) AM/AM of the PA, (b) AM/PM of the PA, (c) AM/AM of the DPD, (d) AM/PM of the DPD.

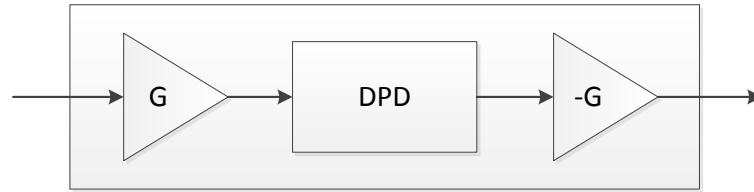


Figure 4.9: Digital predistortion using pre-gain adjustment.

Pre Gain /dB	Output Power /dBm	EVM /dB	ACPR /dB	d /dB
-11	8.66	-52.48	-37.32	7.49
-9	10.66	-52.41	-37.32	7.25
-7	12.66	-52.43	-37.31	7.96
-5	14.66	-52.48	-37.31	7.86
-3	16.66	-52.48	-37.32	8.33
-1	18.66	-46.43	-37.07	6.63
1	20.63	-32.71	-34.02	1.30
3	<i>22.42</i>	<i>-23.81</i>	<i>-28.46</i>	<i>-3.46</i>
5	<i>23.90</i>	<i>-18.71</i>	<i>-23.89</i>	<i>-6.65</i>

Table 4.7: Simulation results of the transmitter without pulse shaping filter using a DPD with 256 entries. (The region where 802.11n is violated is represented italic.)

that the out-of-band distortion is much higher and violate the spectral mask. (c) illustrates the perfect linearized output signal and (d) the linearized output signal with hard clipping. To prevent the PA from clipping the PAPR of the signal have to be reduced to avoid high peaks. Another possibility to avoid the hard clipping is to reduce the linearity of the transmitter and introduce soft clipping.

**Transmitter with pulse shaping filter** The next step is to complete the transmitter by adding the pulse shaping filter again and evaluate the performance of the ideal inverse of the PA and the whole transmitter. Tab. 4.8 shows the performance for different pre-gain levels and Fig. 4.11 illustrate the PSD and the AM/AM of the pre-gain levels -3 and +5 dB. It can be seen that

Pre Gain /dB	Output Power /dBm	EVM /dB	ACPR /dB	d /dB
-11	8.46	-51.79	-39.49	11.35
-9	10.46	-51.53	-39.39	11.33
-7	12.46	-51.24	-39.25	11.31
-5	14.46	-50.43	-39.03	11.36
-3	16.48	-46.54	-38.15	11.22
-1	18.52	-36.19	-33.35	6.62
1	<i>20.60</i>	<i>-29.52</i>	<i>-26.64</i>	<i>-0.94</i>
3	<i>22.56</i>	<i>-23.06</i>	<i>-22.08</i>	<i>-6.95</i>
5	<i>24.15</i>	<i>-18.42</i>	<i>-19.44</i>	<i>-10.72</i>

Table 4.8: Simulation results of the transmitter with pulse shaping filter using a DPD with 256 entries. (The region where 802.11n is violated is represented italic.)

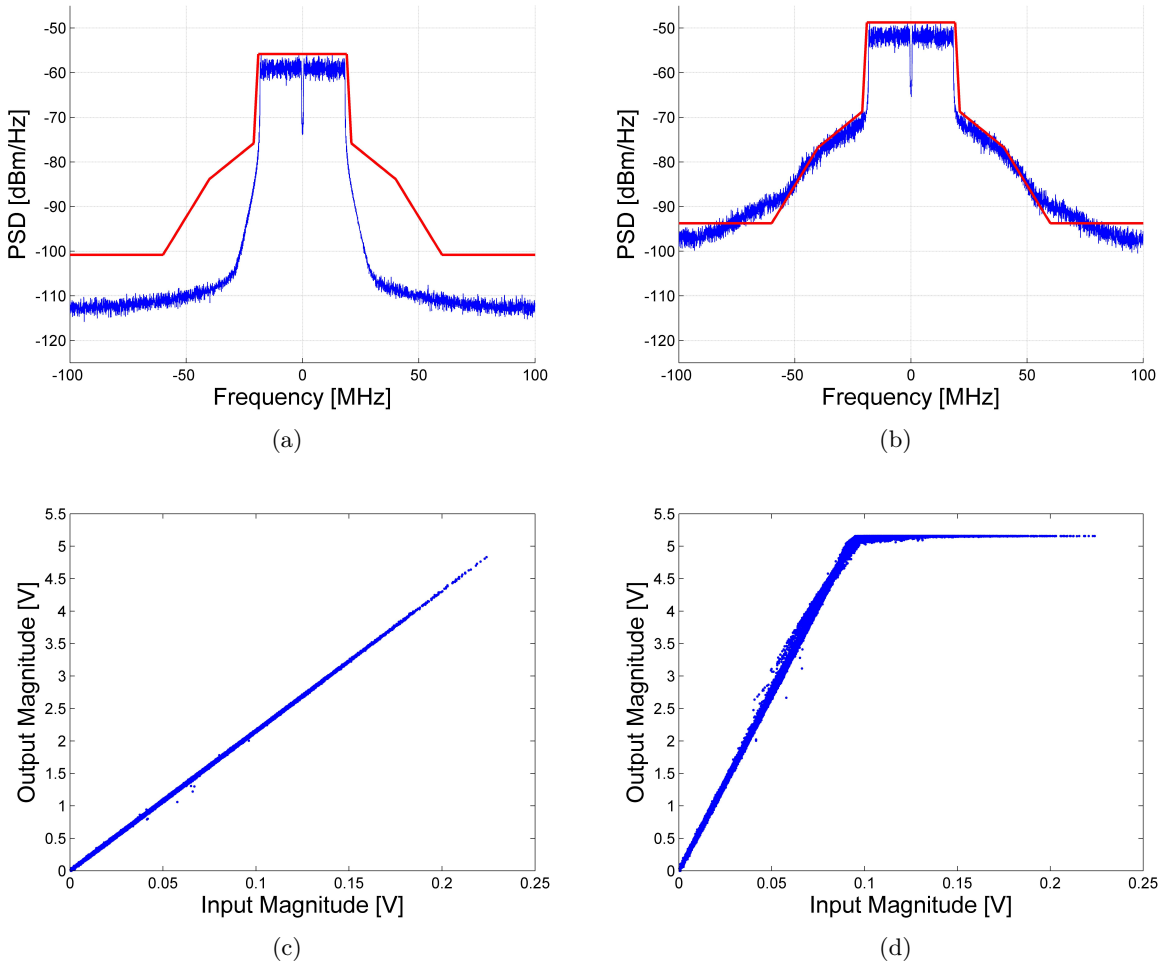


Figure 4.10: Evaluating the output of the ideal transmitter with DPD and pre-gain of (a) PSD: -3 dB, (b) PSD: +5 dB, (c) AM/AM: -3 dB, (d) AM/AM: +5 dB.

the ACPR is better than in Tab. 4.7 for low pre-gain levels, but worse for high levels. The EVM is always worse and the spectral mask is violated for pre-gain levels from 1 dB. As the out-of-band distortions are filtered by the pulse shaping filter the input of the PA is only the in-band-predistorted signal. To allow the compensation of the spectral regrowth the bandwidth of the signal path should be at least five times the signal bandwidth [26, 27]. Therefore the performance of the transmitter with the perfect inverse of the PA which is used as DPD is worse for output powers above 20 dBm than the transmitter without any DPD.

As the transmitter is defined with the pulse shaping filter the next step is to compensate the influence of the pulse shaping filter in-band that the DPD can compensate all effects of the PA in this region.

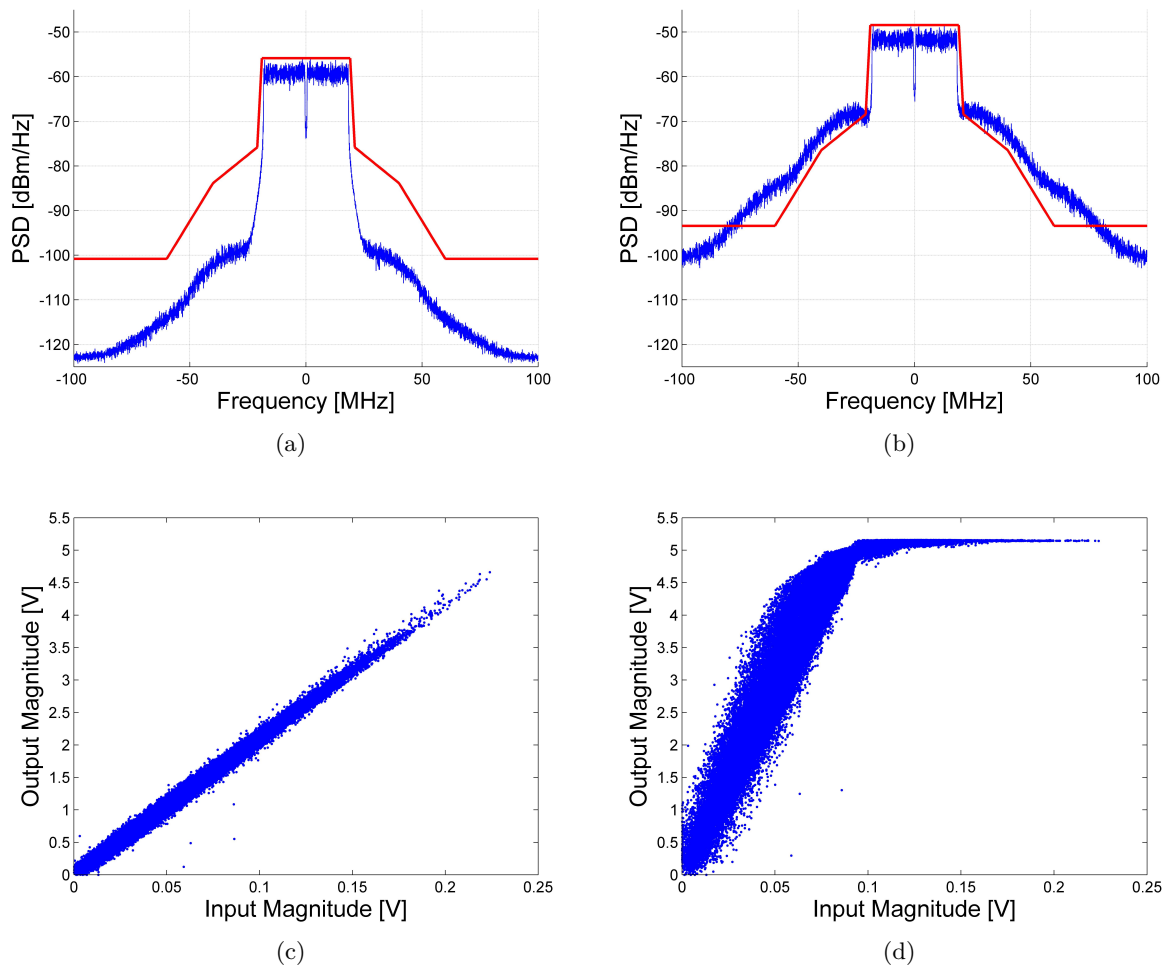


Figure 4.11: Evaluating the output of the ideal transmitter including pulse shaping filter, DPD and pre-gain of (a) PSD: -3 dB, (b) PSD: +5 dB, (c) AM/AM: -3 dB, (d) AM/AM: +5 dB.

### 4.3.3 Ideal Compensation of the Pulse Shaping Filter

The pulse shaping filter is designed to eliminate the distortions above 20 MHz which means the compensation filter should only equalize the in-band-effects whereas the out-of-band behavior is needed for functionality. The compensation filter is designed using the inverse of the frequency response of the filter below 20 MHz and a constant gain of 1 for the out-of-band region. The frequency response of the pulse shaping filter and the inverse is illustrated in Fig. 4.12. For the simulation the compensation filter is placed between DPD and DAC. The output of the transmitter is determined in Tab. 4.9. Compared to the evaluation of the transmitter only using a DPD in Tab. 4.8, the output power is similar weather the ACPR and the EVM are worse. This impairment can be explained by the discontinuity of the transfer function which can be seen in the PSD of the output signal which is illustrated in Fig. 4.13. Inside the frequency band the output signal is compensated but the discontinuity on the edge does produce a worse output.

This result leads to the conclusion that the identification of the pulse shaping filter have to be handled with care. The goal is to find a DPD which compensate in-band distortions because out-of-band distortions which are generated by the DPD will be filtered.

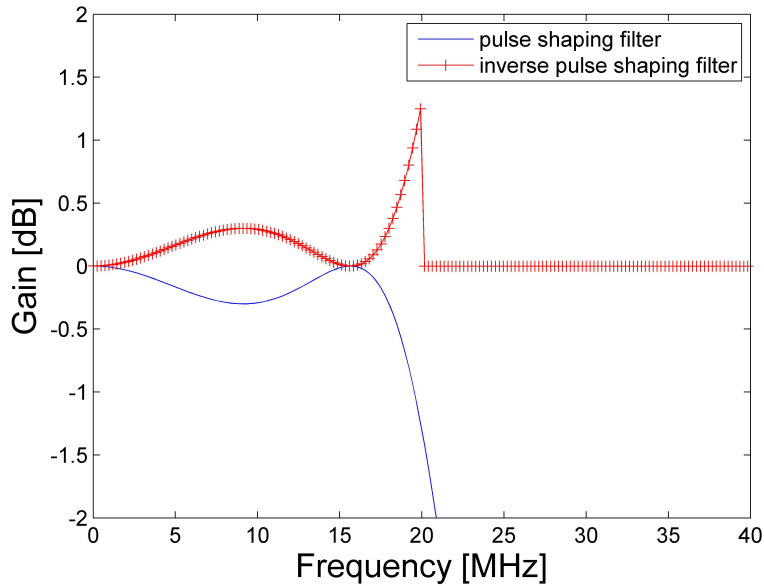


Figure 4.12: Frequency response of the pulse shape filter and the inverse pulse shaping filter

Pre Gain /dB	Output Power /dBm	EVM /dB	ACPR /dB	d /dB
-11	8.69	-45.56	-38.15	10.41
-9	10.69	-45.56	-37.82	10.28
-7	12.69	-45.55	-37.45	10.20
-5	14.69	-45.47	-36.73	9.67
-3	16.70	-43.97	-34.39	7.48
-1	18.78	-31.44	-26.35	-0.82
1	20.97	-25.71	-19.51	-8.14
3	23.02	-20.20	-16.46	-10.51
5	24.57	-17.61	-15.49	-14.17

Table 4.9: Simulation results of the transmitter with a DPD using 256 entries and an ideal pulse shaping compensation filter.

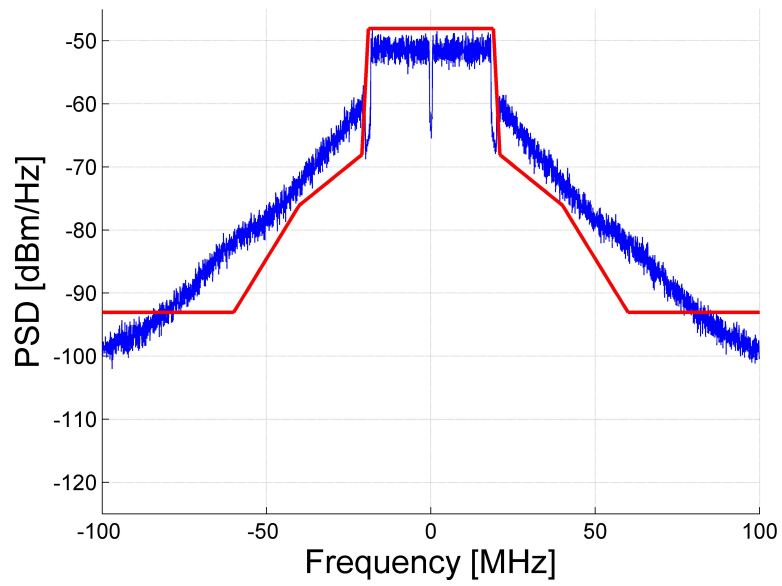


Figure 4.13: PSD of the transmitter using a DPD with 265 entries and an ideal pulse shaping compensation filter.

### 4.3.4 Influence of the Look-up Table Size

When the DPD is implemented on hardware, the LUT is limited in size which may lead to a reduced accuracy. Therefore, the LUT have to be chosen big enough to not introduce additional noise to the system. Fig. 4.14 shows the EVM and ACPR for varying LUT sizes and different pre-gain levels. It can be seen that the improvement by increasing the size is constant in the beginning till a saturation point is reached. Increasing the size of the LUT beyond the saturation point does not necessarily improve the performance. In [28] it is shown that the performance of the LUT can become worse by increasing the table above the saturation point. Tab. 4.10 shows the performance of different LUT sizes for a constant pre-gain factor of -3 dB.

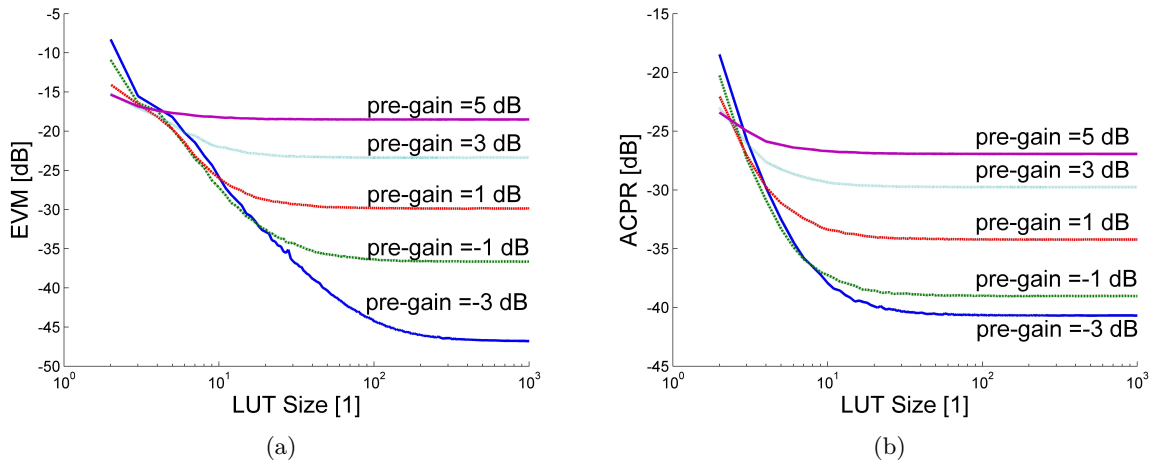


Figure 4.14: Variation of the Look-up table size for different pre-gain levels (a) EVM, (b) ACPR.

LUT Size /Bit	Output Power /dBm	EVM /dB	ACPR /dB	d /dB
2	16.08	-8.29	-18.47	-10.43
4	16.61	-17.02	-29.81	0.68
8	16.36	-23.11	-36.53	6.28
16	16.33	-30.82	-39.42	9.90
32	16.32	-36.96	-40.39	10.64
64	16.32	-42.00	-40.53	11.30
128	16.32	-45.10	-40.64	11.36
256	16.32	-46.25	-40.69	11.44

Table 4.10: Variation of the Look-up table size for constant pre-gain of -3 dB.

One way to increase the performance of a LUT is to use interpolation for finding values between the LUT entries. Fig. 4.15 shows the performance of the LUT using different interpolation techniques. In the hardware an interpolation would require additional computational power wherefore a LUT without interpolation is preferred.

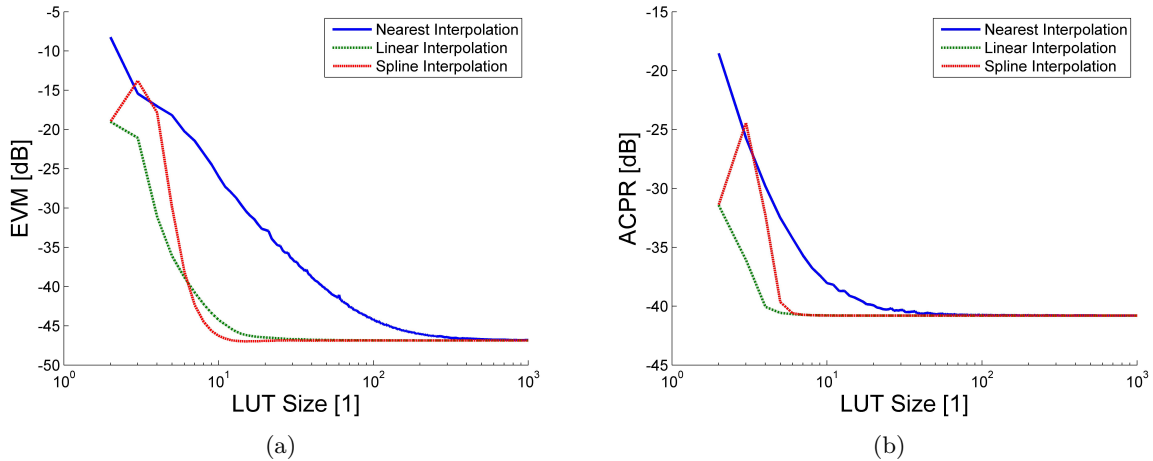


Figure 4.15: Variation of the Look-up table size using different interpolation methods for a constant pre-gain of -3 dB (a) EVM, (b) ACPR.

## 4.4 Identification of the Transmitter

In this section the nonlinearity of the PA will be identified using memoryless models. As the exact characteristic of the PA is known the quality of the identification can be easily determined. The results are shown in tables where the SNR is the main FOM which indicates the performance of the simulated model. The FOMs Power, ACPR and EVM should be the same for the transmitter and the identified transmitter. For all the simulations the pre-gain is set to 3 dB.

**Identification of the PA** As the PA is modeled by a QMM-LUT, the system does include nonlinearity but no memory. Therefore, the identification is performed using a QMM-polynomial and a MLP. The identification is first performed on the transmitter without pulse shaping filter to evaluate the best parameter for the nonlinearity only. In the second stage the PA will be identified using the whole transmitter and the results will be discussed.

**Identification without pulse shaping filter** Tab. 4.11 shows the simulation results for identification of the QMM-polynomial model for different AM/AM and AM/PM orders. It can be seen that the SNR for the simulation using AM/AM-order above 5 and AM/PM-order above 5 does already gives a good SNR. To see how good the polynomials fit to the simulated transmit path the AM/AM and the AM/PM are plotted in Fig. 4.16 where the AM/AM-order 9 and AM/PM order 7 are used. The broadening of the curves is caused by the memory which is introduced by the anti-imaging filter (AIF) of the DAC. The simulation results for the MLP are shown in Tab. 4.12 for different polynomial orders and the MLP of order 9 is plotted in Fig. 4.16. It can be seen that the QMM polynomials gives the better fit to the data then the MLP.

**Identification with pulse shaping filter** To evaluate the influence of the pulse shaping filter the identification is now performed using the whole transmitter where the same nonlinear models are used as found in the identification without pulse shaping filter. The results for the QMM model

$P_{AM/AM}$	$P_{AM/PM}$	Transmitter			Identified Transmitter			d	SNR
		Power	ACPR	EVM	Power	ACPR	EVM		
1	1	21.70	-27.83	-21.51	20.90	-13.48	-13.07	-24.54	7.00
1	3	21.68	-27.76	-21.20	20.87	-13.45	-13.04	-24.63	6.95
1	5	21.69	-27.71	-21.54	20.88	-13.46	-13.05	-24.12	6.98
1	7	21.69	-27.84	-21.54	20.87	-13.40	-13.17	-24.77	6.92
3	1	21.70	-27.93	-21.69	21.70	-27.90	-21.84	1.98	33.80
3	3	21.70	-27.89	-21.52	21.70	-27.70	-21.53	1.61	36.64
3	5	21.69	-27.90	-21.37	21.69	-27.78	-21.43	1.96	37.13
3	7	21.67	-27.62	-21.31	21.67	-27.52	-21.38	2.20	37.11
5	1	21.68	-27.94	-21.43	21.68	-27.93	-21.58	2.75	34.96
5	3	21.70	-27.83	-21.51	21.70	-27.65	-21.51	1.33	39.82
5	5	21.70	-27.86	-21.59	21.70	-27.73	-21.62	1.48	40.94
5	7	21.70	-27.96	-21.39	21.70	-27.82	-21.45	2.54	40.93
7	1	21.70	-28.07	-21.78	21.70	-28.05	-21.95	3.10	35.21
7	3	21.69	-27.76	-21.51	21.69	-27.57	-21.49	1.74	39.73
7	5	21.67	-27.67	-21.38	21.67	-27.53	-21.41	1.90	40.91
7	7	21.67	-27.62	-21.31	21.67	-27.49	-21.35	2.18	40.96
9	1	21.70	-28.07	-21.78	21.70	-28.05	-21.95	3.10	35.18
9	3	21.68	-27.81	-21.22	21.68	-27.62	-21.19	1.89	39.46
9	5	21.68	-27.68	-21.30	21.68	-27.54	-21.33	1.91	40.90
9	7	21.68	-27.74	-21.43	21.68	-27.61	-21.47	2.23	40.94

Table 4.11: Identified transmitter without pulse shaping filter using QMM polynomial.

P	Transmitter			Identified Transmitter			d	SNR
	Power	ACPR	EVM	Power	ACPR	EVM		
1	21.68	-27.80	-21.59	21.63	-36.93	-113.04	8.57	20.08
2	21.70	-27.89	-21.52	21.64	-37.47	-61.26	9.12	20.10
3	21.68	-27.81	-21.22	21.67	-27.65	-21.31	2.02	36.54
4	21.68	-27.81	-21.26	21.68	-27.75	-21.36	2.54	36.73
5	21.67	-27.67	-21.38	21.67	-27.59	-21.46	1.79	38.02
6	21.67	-27.67	-21.38	21.67	-27.59	-21.47	1.80	38.02
7	21.69	-27.85	-21.44	21.69	-27.77	-21.53	1.95	39.01
8	21.70	-27.89	-21.52	21.70	-27.79	-21.61	1.59	39.28
9	21.69	-27.82	-21.54	21.69	-27.70	-21.58	1.82	40.26

Table 4.12: Identified transmitter without pulse shaping filter using MLP.

can be found in Tab. 4.13 and Fig. 4.18 and in Tab. 4.14 and Fig. 4.19 for the MLP model. It can be seen that the LS identification found the same polynomials as in the identification without memory. This proves as well that the pulse shaping filter does not have any nonlinear effect.

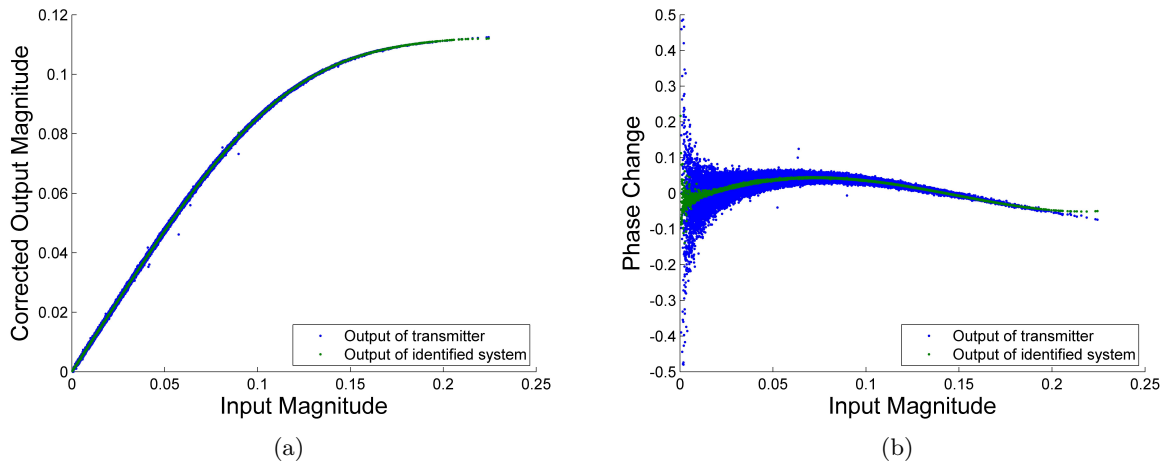


Figure 4.16: Identified transmitter without pulse shaping filter using a QMM polynomial with AM/AM order = 7 and AM/PM order = 5, (a) AM/AM, (b) AM/PM.

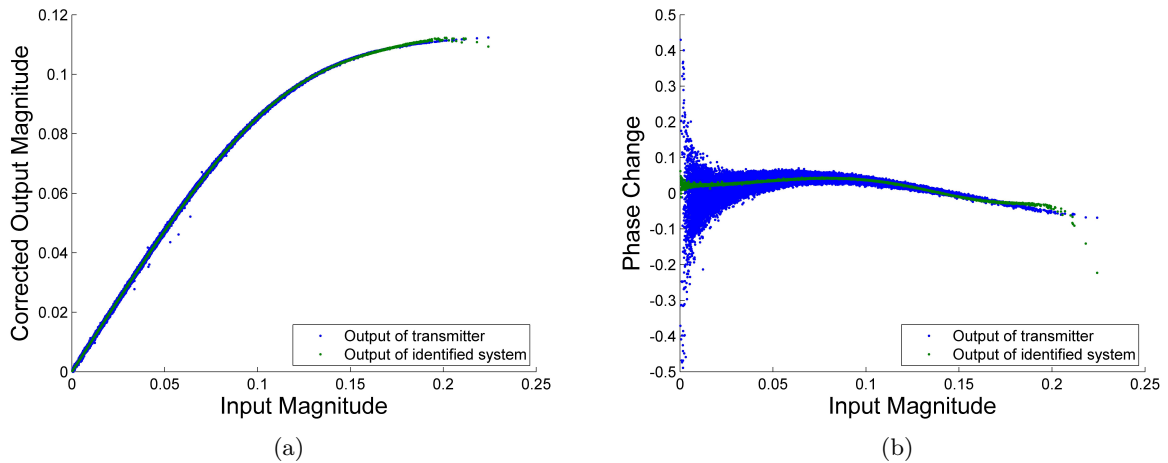


Figure 4.17: Identified transmitter without pulse shaping filter using a MLP with  $P=9$ , (a) AM/AM, (b) AM/PM.

$P_{AM/AM}$	$P_{AM/PM}$	Transmitter			Identified Transmitter			d	SNR
		Power	ACPR	EVM	Power	ACPR	EVM		
7	5	21.54	-28.43	-21.91	21.53	-27.90	-21.91	3.12	24.93

Table 4.13: Identified transmitter using QMM polynomial.

P	Transmitter			Identified Transmitter			d	SNR
	Power	ACPR	EVM	Power	ACPR	EVM		
9	21.55	-28.58	-21.99	21.53	-28.15	-22.10	2.05	24.93

Table 4.14: Identified transmitter using a MLP.

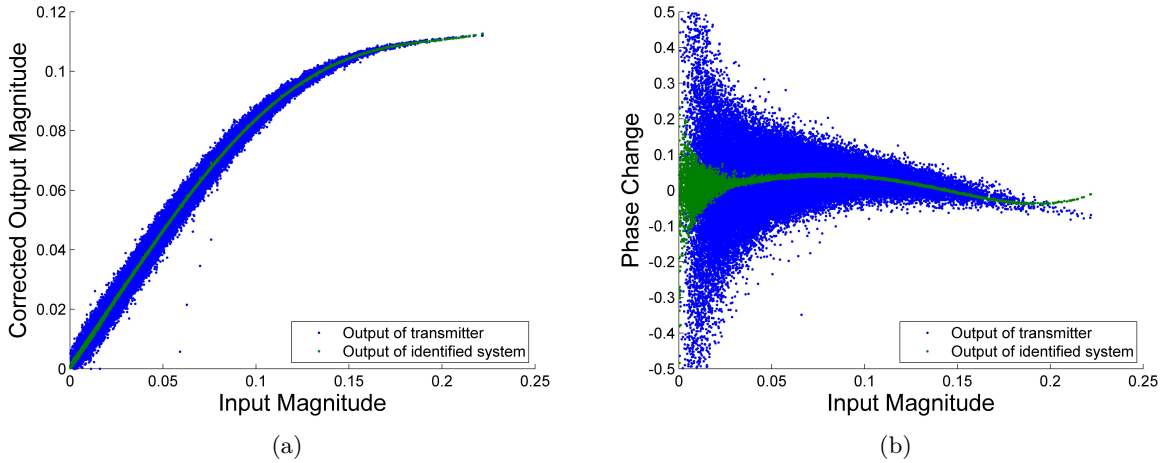


Figure 4.18: Identified transmitter using a QMM polynomial with AM/AM order = 7 and AM/PM order = 5, (a) AM/AM, (b) AM/PM.

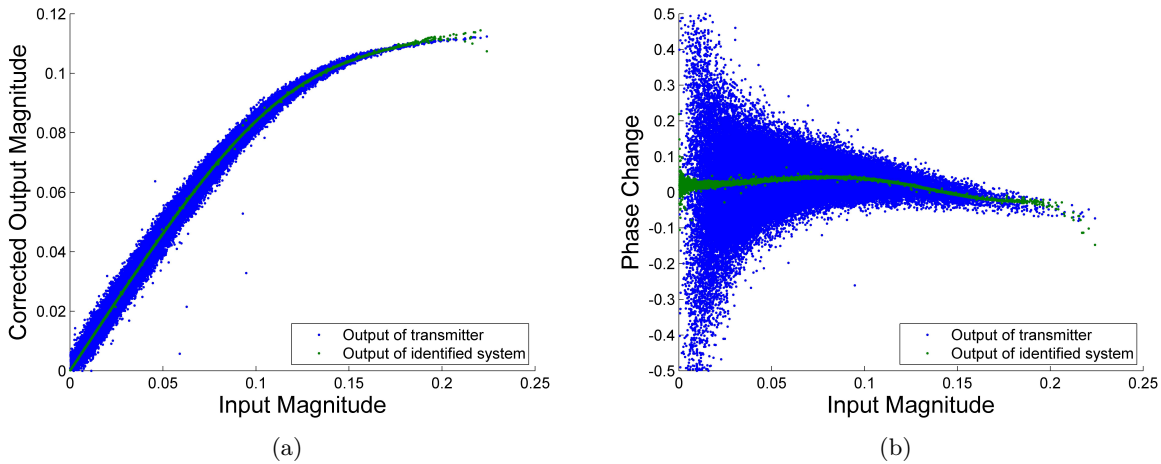


Figure 4.19: Identified transmitter using a MLP with  $P=9$ , (a) AM/AM, (b) AM/PM.

## 4.5 Identification of the DPD

The DPD can be found by identifying the inverse of the transmitter which can be done by switching the in- and output signal for the identification. As the transmitter consists of a pulse shaping filter which only introduce memory and the PA which only introduce nonlinearity the two parts will be identified separately first. The results of the identified PA can be compared with them from Section 4.3.2 where the DPD was created by inverting the PA model. Next a DPD of the whole transmitter will be created by identifying the transmitter using a nonlinear model with memory.

To evaluate the complexity of the system the number of independent parameter  $N$  will be evaluated for all the simulations. The identification of the DPD is performed as defined in Section 4.3.2 for a pre-gain of 0 dB weather the pre-gain is set to -3 dB for the verification which is enough for an output power of  $\sim 17$  dB and does avoid clipping. In the last part of this section

the DPD is evaluated for higher pre-gain levels.

#### 4.5.1 Identification of the Inverse Nonlinearity

The performance of the identification using QMM polynomials is shown in Tab. 4.15. It can be seen that the usage of a DPD increase the EVM for more than 10 dB by keeping the ACPR on the same level. Furthermore the output power is increased. The increase of the performance can also be seen in Fig. 4.20 where the AM/AM, the AM/PM and the PSD is shown for the scenario with  $P_{AM/AM} = 7$  and  $P_{AM/PM} = 7$ . The identification of the transmitter using a MLP is shown in Tab. 4.16 and depicts that the same performance can be achieved by using less parameter.

$P_{AM/AM}$	$P_{AM/PM}$	N	Transmitter				With DPD			
			Power	ACPR	EVM	d	Power	ACPR	EVM	d
1	1	2	16.33	-37.49	-34.95	10.98	17.97	-21.27	-13.93	-5.98
1	3	4	16.33	-37.10	-34.94	10.09	17.92	-21.42	-13.86	-6.83
1	5	6	16.32	-37.18	-34.72	9.83	17.96	-21.27	-13.84	-6.72
1	7	8	16.33	-36.83	-34.93	9.67	17.94	-21.20	-13.81	-6.93
3	1	4	16.33	-37.33	-35.05	10.21	16.72	-37.50	-37.47	9.97
3	3	6	16.33	-37.29	-35.07	10.52	16.72	-37.79	-40.18	10.08
3	5	8	16.33	-37.14	-34.96	10.19	16.71	-37.63	-40.39	10.62
3	7	10	16.33	-37.08	-35.13	9.49	16.71	-37.51	-40.29	10.05
5	1	6	16.33	-37.46	-35.19	9.65	16.73	-37.63	-39.90	9.98
5	3	8	16.33	-37.05	-35.05	8.78	16.74	-37.41	-48.03	9.10
5	5	10	16.32	-37.23	-34.99	9.52	16.73	-37.73	-48.70	10.01
5	7	12	16.32	-37.20	-34.73	9.22	16.74	-37.30	-40.29	9.42
7	1	8	16.32	-37.14	-34.47	9.21	16.73	-37.00	-39.74	9.87
7	3	10	16.32	-37.38	-34.79	10.57	16.74	-37.80	-48.23	10.39
7	5	12	16.33	-37.32	-35.02	10.17	16.73	-37.72	-47.53	10.26
7	7	14	16.33	-37.61	-35.19	9.87	16.73	-38.12	-48.25	9.83
9	1	10	16.32	-37.46	-34.75	10.15	16.74	-37.45	-39.72	10.33
9	3	12	16.33	-37.26	-35.05	10.08	16.73	-37.65	-48.16	10.29
9	5	14	16.33	-37.69	-35.27	11.28	16.73	-38.15	-48.59	10.61
9	7	16	16.33	-37.31	-34.95	10.25	16.73	-37.72	-47.89	10.45

Table 4.15: Transmitter w/o and w/ QMM-polynomials-DPD.

P	N	Transmitter				With DPD			
		Power	ACPR	EVM	d	Power	ACPR	EVM	d
3	3	16.32	-37.27	-35.01	9.80	16.96	-37.01	-37.99	9.20
5	5	16.33	-37.31	-34.93	10.04	17.00	-37.32	-46.46	10.39
7	7	16.33	-37.29	-34.84	9.97	16.99	-37.46	-46.58	9.86
9	9	16.33	-37.54	-34.90	10.89	17.00	-37.63	-47.86	10.20

Table 4.16: Transmitter w/o and w/ MLP-DPD.

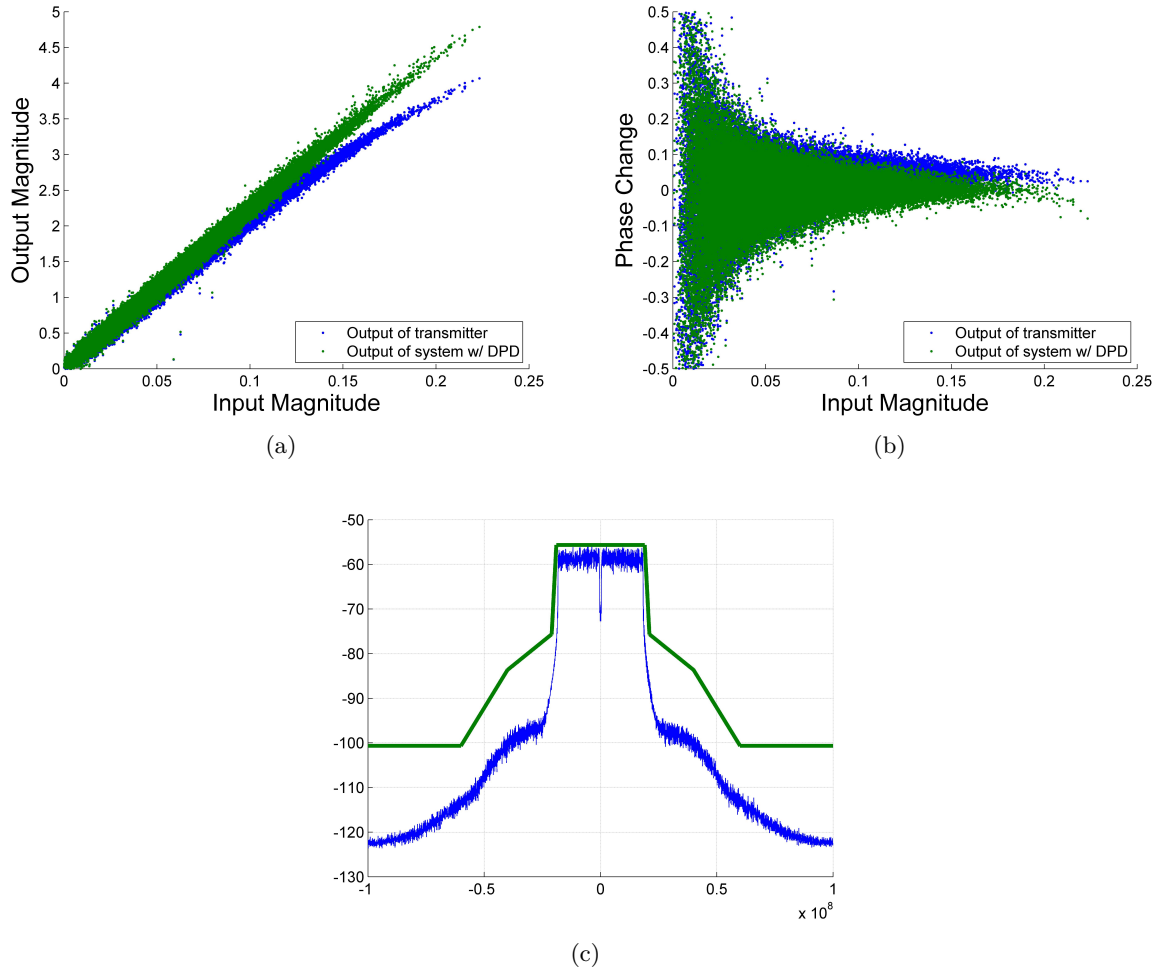


Figure 4.20: Transmitter w/ QMM-polynomial-DPD,  $P_{AM/AM} = 7$ ,  $P_{AM/PM} = 7$ , (a) AM/AM, (b) AM/PM, (c) PSD.

#### 4.5.2 Identification of the Inverse Memory

The next step is to identify the memory of the transmitter which is done by identifying a linear filter of the transmitter. The frequency response of the filter using a memory of 30 and a pre-gain of 0 dB is shown in Fig. 4.21(a). To reduce the influence of the PA the pre-gain is set to -11 dB in the next simulation that the PA is used in the linear region which is illustrated in (b). (c) shows the identification without PA. It can be seen that the inverse of the pulse shaping filter can be identified up to a certain frequency for the simulation without PA. This compensation allows a better compensation of the nonlinearity of the PA as the total signal bandwidth is increased and therefore the spectral broadening of the PA can be compensated by the DPD. The drawback of the compensation is that the linear filter does have a high out-of-band gain wherefore it cannot be implemented in hardware. Therefore, the usage of a system where the nonlinearity and the memory are identified separately will no longer be discussed.

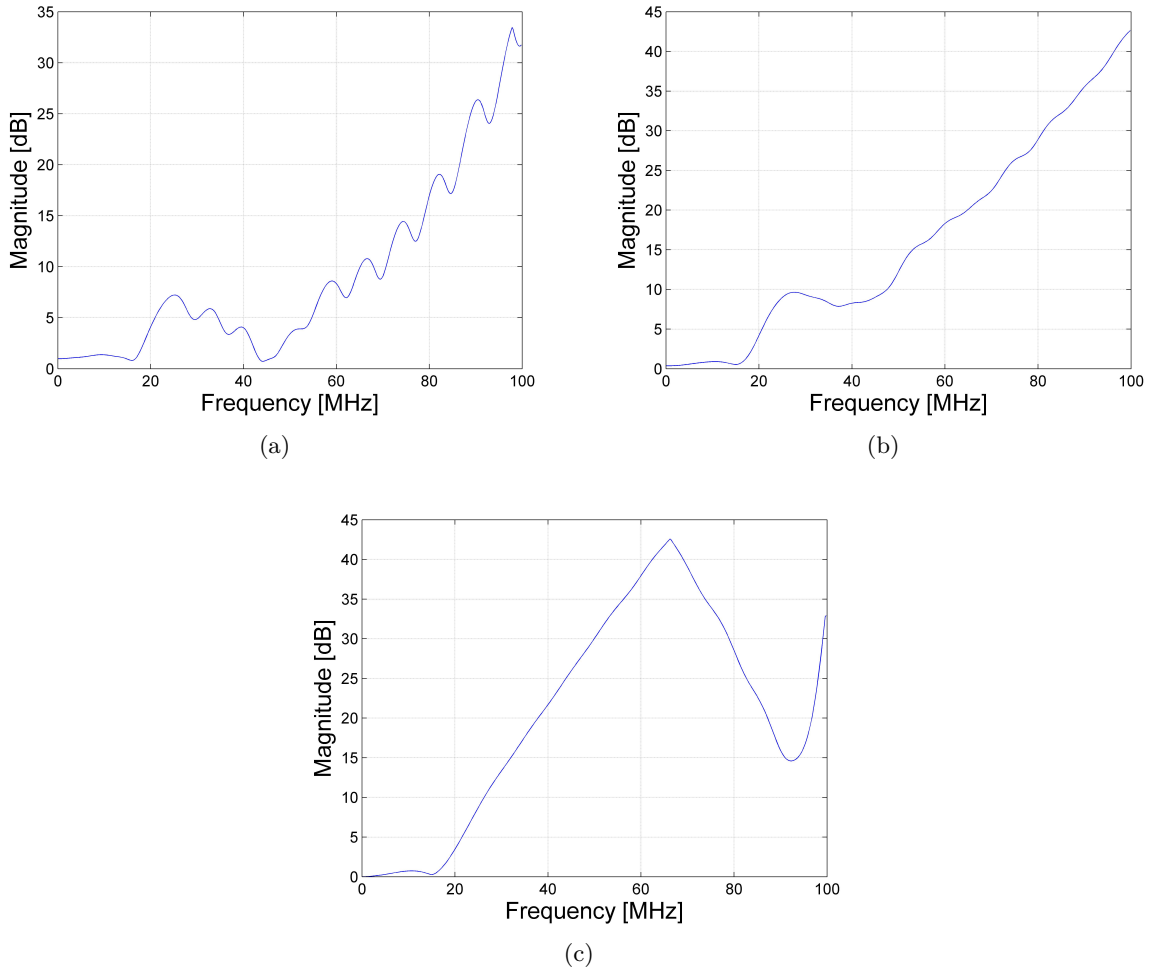


Figure 4.21: Frequency response of the identified linear filter of the transmitter (a) with pre-gain = 0 dB, (b) pre-gain = -11 dB, (c) w/o PA.

### 4.5.3 Identification of the Inverse Transmitter

The DPD of the transmitter can be created by either separately identifying the memory and the nonlinearity and combining the results to a wiener system or by identifying the both things at the same time by using a nonlinear model with memory. As discussed in the last section the inverse of the pulse shaping filter would compensate the out-of-band behavior of the filter which is required for functionality. Therefore, this section only elaborates the identification of the transmitter using a nonlinear model with memory.

**Volterra series** To limit the complexity of the system the number of independent parameter of the Volterra series is set to 30. Another requirement to the model is that a higher order does not have more memory than lower orders. Using these two conditions 64 possible realizations can be found. A list with all the realizations can be found in Appendix A. The results of the 10 models which produced the best results for the DPD are shown in Tab. 4.17. It can be seen that the best solutions are the one where all the orders are present whereby the memory is small for higher orders. To reduce the amount of parameter a MP is used in the next step.

Model	Transmitter				With DPD			
	Power	ACPR	EVM	d	Power	ACPR	EVM	d
V1	16.33	-37.49	-34.95	10.98	16.99	-37.72	-46.86	11.14
V55	16.33	-37.61	-35.22	10.17	16.98	-35.7	-46.22	7.49
V57	16.33	-37.34	-35.02	10.27	16.98	-35.31	-45.79	8.04
V38	16.33	-37.23	-35.12	10.11	16.98	-35.56	-45.74	8.19
V42	16.33	-37.23	-35.01	9.43	16.98	-35.36	-45.71	7.15
V43	16.33	-37.43	-35.14	10.53	16.98	-35.55	-45.65	7.8
V46	16.33	-36.92	-35.12	9.29	16.98	-34.97	-45.61	7.57
V52	16.33	-37.44	-34.96	10.61	16.98	-35.51	-45.58	8.1
V59	16.33	-37.26	-34.96	9.79	16.98	-35.22	-45.53	7.23
V49	16.33	-37.4	-34.98	9.73	16.98	-35.6	-45.5	8.12

Table 4.17: Identified DPD using a Volterra series with 30 coefficients.

**Memory polynomial** As elaborated in the section above the DPD should have at least an order of  $P = 7$ . Therefore the MP is evaluated using the orders  $P = 7$  and  $P = 9$  where all orders does have the same memory. The results of this simulation can be found in Tab. 4.18. It can be seen that a MP can increase the performance of the DPD as compared to the QMM-polynomial from Tab. 4.15. To further investigate the MP found for  $P = 9$  and  $M = 2$ , the frequency response of the first order is illustrated in Fig. 4.22. It can be seen that the memory does compensate the pulse shaping filter which is already discussed in Section 4.5.2. Therefore, the best result for the DPD can be achieved by using a memoryless model.

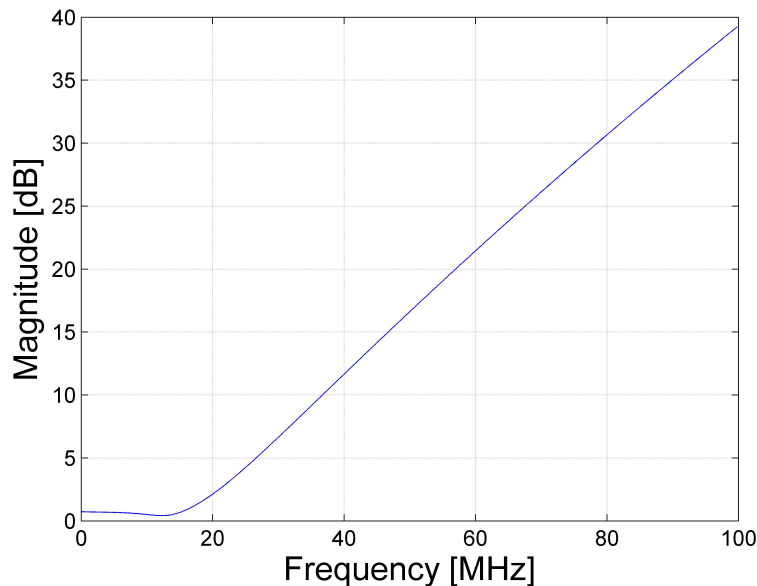


Figure 4.22: Frequency response of the first order of the MP-DPD with  $P=9$ ,  $M=2$ .

P	M	N	Transmitter				With DPD			
			Power	ACPR	EVM	d	Power	ACPR	EVM	d
7	0	7	16.32	-37.29	-35.06	9.95	17.00	-37.46	-47.50	10.48
7	1	14	16.33	-37.03	-35.03	9.76	17.00	-37.16	-47.79	10.42
7	2	21	16.32	-37.58	-34.87	10.70	16.99	-37.77	-47.45	9.97
7	3	28	16.32	-36.88	-34.66	9.02	17.00	-36.59	-48.17	8.46
9	0	9	16.32	-37.13	-34.80	9.54	17.00	-37.18	-47.62	9.86
9	1	18	16.33	-36.99	-34.97	9.50	16.99	-37.19	-48.09	9.54
9	2	27	16.33	-37.22	-34.71	10.50	16.99	-37.48	-47.86	10.79
9	3	36	16.33	-37.34	-35.08	9.23	17.00	-37.14	-49.64	8.71

Table 4.18: Transmitter w/o and w/ MP-DPD.

#### 4.5.4 Performance of the DPD for High Output Power

The goal of this section is to find a DPD for the transmitter to achieve an output power of about 19 dBm. To get this output power the transmitter cannot be used in the linear range any more as the output power of the PA is too low (see Section 4.2 on page 30). For the identification of the nonlinearity for high gain, the pre-gain during the identification is always set 2 dB above the pre-gain of the evaluation to ensure the whole input range of the PA is known. Therefore, the highest pre-gain used for this simulation is +3 dB.

As in the previous part of this section elaborated, the QMM-polynomial gives good results for the DPD. The transmitter now is evaluated for different pre-gains and a QMM polynomial-DPD where  $P_{AM/AM} = 7$  and  $P_{AM/PM} = 7$ . The result is shown in Tab. 4.19 and Fig. 4.23. It can be seen that the DPD increase the performance of the transmitter for pre-gain levels below -1 dB. For -1 dB the EVM is almost the same, but the output power could be increased using the DPD which is enough for the output power of  $\sim 19$  dBm. For higher pre-gain levels the DPD cause a worsening of the signal quality. This is caused on the one hand on the polynomial identification which cannot fit the steep slope of the inverse when the PA is used in saturation and on the other hand on the limitations of the pulse shaping filter and the limited output power of the PA. It can be seen that transmitter can reach a higher output power without violating the requirements if the identified DPD is not used. Therefore, a more sophisticated identification method must be found for high output powers above 19 dBm to achieve the performance which would be possible as shown in Tab. 4.8 .

**Performance without pulse shaping filter** This part evaluates the performance which could be achieved if the pulse shaping filter need not to be compensated which could be implemented in future transmitter. Therefore, the pulse shaping filter is shifted to the signal generator. Tab. 4.20 and Fig. 4.24 shows that the EVM can be decreased up to a pre-gain level of 1 dB by using a QMM polynomial. For an output power at about 19 dBm the EVM can be decreased for  $\sim 14$  dB. The drawback of the DPD is that the mask distance decrease- and the EVM increase faster when the limit of the PA is reached and hard clipping occurs. The simulation results of the MP-DPD with order 9 and a memory of 2 are shown in Tab. 4.21 and Fig. 4.25. It can be seen that the EVM could be decreased below -25 dB for an output power of 20.68 dB,

pre-gain	Transmitter				With DPD			
	Power	ACPR	EVM	d	Power	ACPR	EVM	d
-11	8.46	-38.67	-40.06	10.63	8.73	-39.03	-50.37	10.81
-9	10.45	-38.19	-39.30	10.03	10.72	-38.57	-50.01	10.17
-7	12.44	-38.21	-38.45	11.05	12.73	-38.67	-50.78	11.22
-5	14.40	-37.33	-37.32	9.54	14.73	-37.82	-50.43	9.74
-3	16.32	-37.35	-34.82	9.45	16.73	-37.74	-46.10	10.08
-1	18.19	-35.43	-31.11	9.00	18.75	-32.59	-30.19	7.54
1	19.93	-32.06	-26.17	6.61	<i>20.80</i>	<i>-23.92</i>	<i>-20.98</i>	<i>-4.84</i>
3	<i>21.52</i>	<i>-28.32</i>	<i>-21.64</i>	<i>2.55</i>	<i>22.85</i>	<i>-18.63</i>	<i>-18.25</i>	<i>-14.45</i>

Table 4.19: Transmitter w/o and w/ QMM-polynomial-DPD ( $P_{AM/AM} = 7$ ,  $P_{AM/PM} = 7$ ) for differend pre-gain levels. (The region where 802.11n is violated is represented italic.)

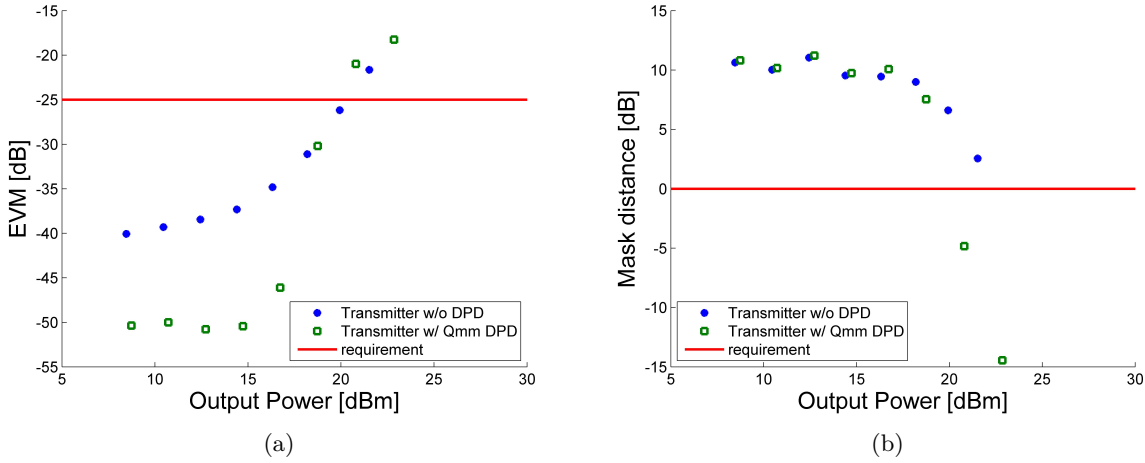


Figure 4.23: Transmitter w/ pulse shaping filter, w/ and w/o QMM-DPD ( $P_{AM/AM} = 7$ ,  $P_{AM/PM} = 7$ ), (a) EVM, (b) Mask distance.

pre-gain	Transmitter				With DPD			
	Power	ACPR	EVM	d	Power	ACPR	EVM	d
-11	8.66	-35.94	-39.99	7.52	8.73	-36.34	-52.44	7.69
-9	10.65	-35.96	-39.15	6.76	10.73	-36.52	-52.50	7.86
-7	12.64	-36.20	-38.35	6.03	12.73	-36.89	-52.37	7.47
-5	14.60	-36.41	-37.32	6.69	14.73	-37.44	-52.44	8.02
-3	16.51	-35.45	-34.28	5.73	16.73	-36.99	-52.61	7.66
-1	18.37	-33.74	-30.45	5.04	18.73	-36.36	-44.83	6.55
1	20.10	-30.99	-25.72	5.69	<i>20.68</i>	<i>-25.69</i>	<i>-22.43</i>	<i>-12.02</i>
3	<i>21.69</i>	<i>-28.03</i>	<i>-21.50</i>	<i>1.90</i>	<i>22.47</i>	<i>-16.28</i>	<i>-16.48</i>	<i>-22.73</i>

Table 4.20: Transmitter w/o pulse shaping filter, w/o and w/ QMM-polynomial-DPD ( $P_{AM/AM} = 7$ ,  $P_{AM/PM} = 7$ ) for differend pre-gain levels. (The region where 802.11n is violated is represented italic.)

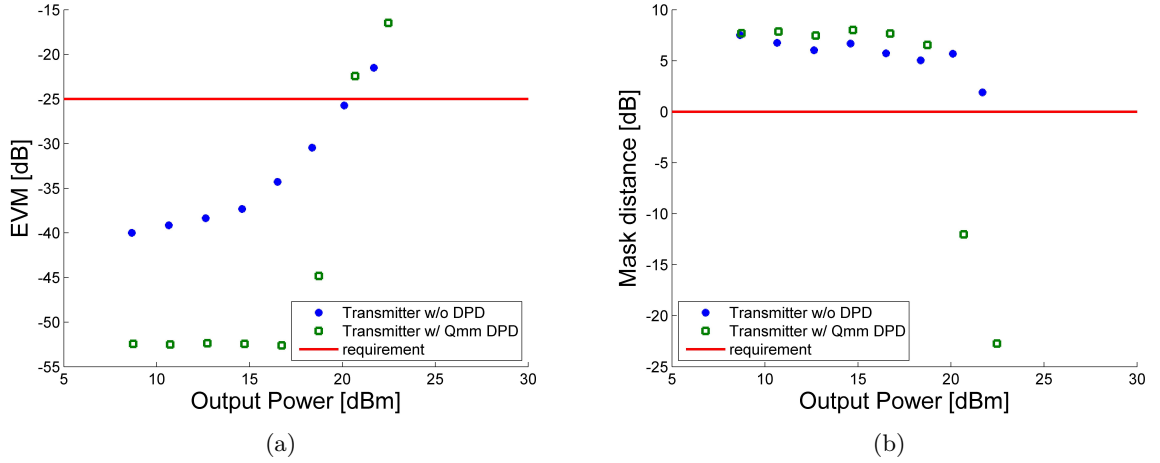


Figure 4.24: Transmitter w/o pulse shaping filter, w/ and w/o QMM-DPD ( $P_{AM/AM} = 7$ ,  $P_{AM/PM} = 7$ ), (a) EVM, (b) Mask distance.

but the mask is still violated.

pre-gain	Transmitter				With DPD			
	Power	ACPR	EVM	d	Power	ACPR	EVM	d
-11	8.66	-36.46	-40.07	7.56	8.73	-36.77	-52.25	7.53
-9	10.65	-36.36	-39.14	7.02	10.73	-36.73	-52.13	7.93
-7	12.63	-35.81	-38.30	6.91	12.73	-36.26	-52.06	7.43
-5	14.60	-35.81	-37.14	6.76	14.73	-36.48	-51.96	7.36
-3	16.52	-35.22	-34.77	6.51	16.73	-36.42	-51.95	7.80
-1	18.37	-33.89	-30.62	5.73	18.73	-36.52	-43.33	4.72
1	20.11	-31.26	-25.76	5.38	<i>20.68</i>	<i>-31.38</i>	<i>-29.56</i>	<i>-5.31</i>
3	<i>21.69</i>	<i>-27.89</i>	<i>-21.70</i>	<i>2.54</i>	<i>22.49</i>	<i>-24.43</i>	<i>-20.36</i>	<i>-12.14</i>

Table 4.21: Transmitter without pulse shaping filter, w/o and w/ MP-DPD ( $P = 9$ ,  $M = 2$ ) for different pre-gain levels. (The region where 802.11n is violated is represented italic.)

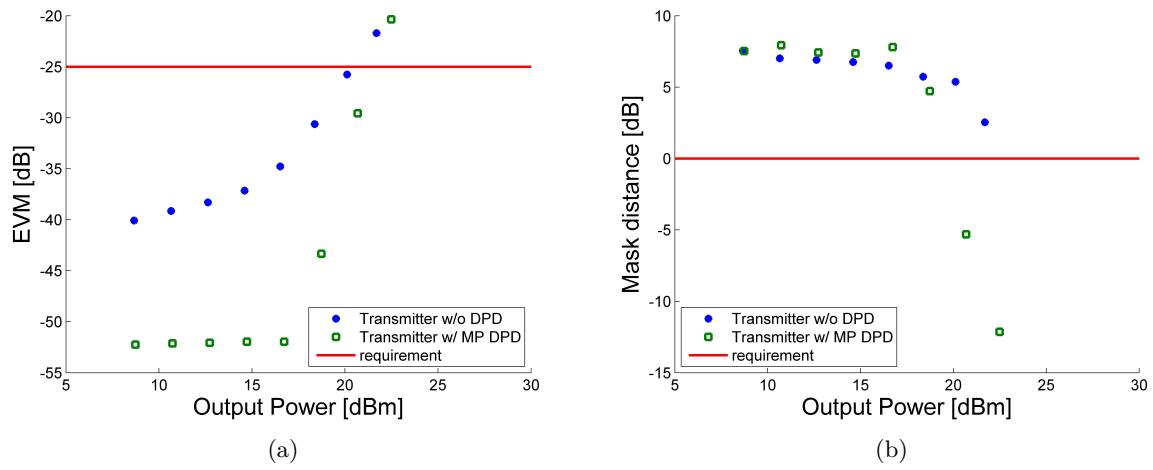


Figure 4.25: Transmitter w/o pulse shaping filter, w/ and w/o MP-DPD ( $P = 9$ ,  $M = 2$ ), (a) EVM, (b) Mask distance.

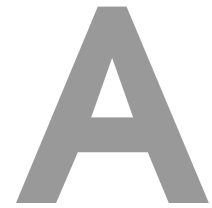
# 5

## Conclusion

This thesis investigated the performance of the identification and the DPD for a given WLAN transmitter. Within the work following things were shown:

- It is shown that a DPD can be found to increase the performance of the transmitter up to the maximal output power for a perfectly linearized transmitter. For higher output powers hard clipping occurs which can introduce more distortions than in the transmitter without DPD. To further increase of the performance soft clipping can be introduced to ensure a smooth transition between the linear amplification and the saturation.
- The DPD can not exploit the whole potential as it is band limited by the pulse shaping filter. If the filter would be shifted to the signal generator the DPD would also be capable of compensating the spectral broadening of the PA.
- The LS identification of the DPD with memory does use the memory to compensate the out-of-band attenuation of the pulse shaping filter. Therefore, the identified DPD does have a high out-of-band gain which can not be implemented for real systems.
- The best DPD which was found to linearize the given transmitter can be implemented using a QMM which can be easily performed on hardware.





# Volterra Models

Nr.	Memory in Order								
	1	2	3	4	5	6	7	8	9
V1	3	3	2	2	1	1	1	0	0
V2	3	3	3	0	0	0	0	0	0
V3	4	3	2	2	1	1	0	0	0
V4	4	4	2	1	1	1	1	0	0
V5	5	3	2	2	1	0	0	0	0
V6	5	4	2	1	1	1	0	0	0
V7	5	5	0	0	0	0	0	0	0
V8	6	2	2	2	1	1	1	1	1
V9	6	3	2	2	0	0	0	0	0
V10	6	4	2	1	1	0	0	0	0
V11	7	2	2	2	1	1	1	1	0
V12	7	4	1	1	1	1	1	1	1
V13	7	4	2	1	0	0	0	0	0
V14	8	2	2	2	1	1	1	0	0
V15	8	4	1	1	1	1	1	1	0
V16	8	4	2	0	0	0	0	0	0
V17	9	2	2	2	1	1	0	0	0
V18	9	3	2	1	1	1	1	1	1
V19	9	4	1	1	1	1	1	0	0
V20	10	2	2	2	1	0	0	0	0
V21	10	3	2	1	1	1	1	1	0
V22	10	4	1	1	1	1	0	0	0
V23	11	2	2	2	0	0	0	0	0
V24	11	3	2	1	1	1	1	0	0
V25	11	4	1	1	1	0	0	0	0
V26	12	3	2	1	1	1	0	0	0
V27	12	4	1	1	0	0	0	0	0
V28	13	3	2	1	1	0	0	0	0
V29	13	4	1	0	0	0	0	0	0
V30	14	2	2	1	1	1	1	1	1
V31	14	3	1	1	1	1	1	1	1
V32	14	3	2	1	0	0	0	0	0
V33	14	4	0	0	0	0	0	0	0
V34	15	2	2	1	1	1	1	1	0
V35	15	3	1	1	1	1	1	1	0
V36	15	3	2	0	0	0	0	0	0

V37	16	2	2	1	1	1	1	0	0
V38	16	3	1	1	1	1	1	0	0
V39	17	2	2	1	1	1	0	0	0
V40	17	3	1	1	1	1	0	0	0
V41	18	2	2	1	1	0	0	0	0
V42	18	3	1	1	1	0	0	0	0
V43	19	2	1	1	1	1	1	1	1
V44	19	2	2	1	0	0	0	0	0
V45	19	3	1	1	0	0	0	0	0
V46	20	2	1	1	1	1	1	1	0
V47	20	2	2	0	0	0	0	0	0
V48	20	3	1	0	0	0	0	0	0
V49	21	2	1	1	1	1	1	0	0
V50	21	3	0	0	0	0	0	0	0
V51	22	1	1	1	1	1	1	1	1
V52	22	2	1	1	1	1	0	0	0
V53	23	1	1	1	1	1	1	1	0
V54	23	2	1	1	1	0	0	0	0
V55	24	1	1	1	1	1	1	0	0
V56	24	2	1	1	0	0	0	0	0
V57	25	1	1	1	1	1	0	0	0
V58	25	2	1	0	0	0	0	0	0
V59	26	1	1	1	1	0	0	0	0
V60	26	2	0	0	0	0	0	0	0
V61	27	1	1	1	0	0	0	0	0
V62	28	1	1	0	0	0	0	0	0
V63	29	1	0	0	0	0	0	0	0
V64	30	0	0	0	0	0	0	0	0

Table A.1: Possible realizations of a volterra series with order = 9 and 30 independent coefficients.



## Glossary

802.11ac	IEEE 802.11ac 2, 4, 5
802.11n	IEEE 802.11n 1, 2, 4, 5
ACPR	adjacent channel power ratio 29, 32, 33, 38, 39, 42, 43, 47
ADC	analog to digital converter 35
AIF	anti-imaging filter 43
AM/AM	AM/AM conversation 18, 19, 28, 30, 32, 33, 35, 37, 43, 47
AM/PM	AM/PM conversation 18, 19, 28, 30, 32, 33, 35, 43, 47
DAC	digital to analog converter 8–10, 33, 35, 39, 43, 61
DPD	digital predistortion 1, 10, 14, 27, 31, 35, 38, 39, 42, 46–51, 55
EVM	error vector magnitude 2, 5, 27, 29, 32, 33, 35, 38, 39, 42, 43, 47, 51
FFT	fast Fourier transformation 28
FIR	finite impulse response 8
FOM	figures of merit 27, 43
HF	high frequency 10
I/O	input/output 15, 18, 21, 28, 32
ICI	interchannel interference 4
ISI	intersymbol interference 2
LMS	least mean squares 23
LP	low pass 8, 9
LS	least squares 23–25, 27, 44, 55
LTI	linear time-invariant 12, 15
LUT	Look-up table 18, 19, 30, 31, 35, 42, 43
MLP	memoryless polynomial 17, 18, 43, 44, 47
MP	memory polynomial 18, 49–51

MATLAB	MathWorks MATLAB© 2, 8, 24, 28, 31
OFDM	orthogonal frequency division multiplexing 1–3, 5, 8, 27, 29
PA	power amplifier 1, 7, 10, 11, 14, 15, 18, 19, 22, 23, 27, 30–33, 35, 37, 38, 43, 46, 48, 51, 55, 61
PAPR	peak-to-average power ratio 1, 29, 30, 37
PSD	power spectral density 8, 28, 35, 37, 39, 47
QMM	Quasi-memoryless 18, 19, 30, 32, 35, 43, 47, 50, 51, 55
RBW	resolution bandwidth 28
RCE	relative constellation error 5
RF	radio frequency 7, 11, 12, 14, 17
RFIC	radio frequency integrated circuit 1, 30
RMS	root mean square 5, 28, 29
SNR	signal to noise ratio 29, 43
VNA	vector network analyzer 18
WLAN	wireless local area network 1, 2, 4, 8, 9, 55

## List of Figures

1.1	Subcarriers of an OFDM signal. . . . .	3
1.2	Transmit spectral mask definition in 802.11n. . . . .	4
2.1	Block diagram of a transmitter [8] . . . . .	7
2.2	Block diagram of a WLAN transmitter . . . . .	8
2.3	PSD of the (a) OFDM signal, (b) upsampled OFDM signal. . . . .	9
2.4	Block diagram of a DAC . . . . .	9
2.5	Typical AM/AM characteristic of a PA . . . . .	11
2.6	Frequency spectrum of RF- and Baseband model: (a) RF (b) Baseband . . . . .	11
2.7	Frequency spectrum of a simple nonlinearity: (a) $\mathcal{F}\{x(t)\}$ (b) $\mathcal{F}\{x^2(t)\}$ , $\mathcal{F}\{x^3(t)\}$ . . . . .	13
2.8	Zones in the frequency band. . . . .	14
2.9	Baseband model of a transmitter using identification and DPD . . . . .	14
2.10	Schematic representation of a volterra series. . . . .	16
3.1	Preprocessing block. . . . .	21
3.2	Illustration of a time delay. . . . .	22
3.3	AM/AM characteristic with different gain-factors: (a) Maximum Linearity Estimation (b) Maximum Gain Estimation . . . . .	22
3.4	Compensation of a phase shift: (a) before compensation, (b) after compensation. . . . .	23
3.5	Basic structure of a identification process. . . . .	24
4.1	Error vector of an OFDM symbol. . . . .	29
4.2	Main- and Adjacent channel. . . . .	30
4.3	Characteristic of the PA model (a) AM/AM, (b) AM/PM. . . . .	31
4.4	PSD of the transmitter without DPD and pre-gain of (a) -3 dB, (b) +5 dB. . . . .	32
4.5	Evaluating influences of transmitter in time domain without DPD and pre-gain of (a) AM/AM: -3 dB, (b) AM/PM: -3 dB, (c) AM/AM: +5 dB, (d) AM/PM: +5 dB. . . . .	33
4.6	Transmitter without pulse shaping filter, DPD and a pre-gain of +5 dB (a) AM/AM, (b) AM/PM, (c) PSD. . . . .	34
4.7	Principle amplitude distortion in DPD. . . . .	36
4.8	Amplitude- and Phase characteristic of the normalized PA and the DPD (a) AM/AM of the PA, (b) AM/PM of the PA, (c) AM/AM of the DPD, (d) AM/PM of the DPD. . . . .	36
4.9	Digital predistortion using pre-gain adjustment. . . . .	37
4.10	Evaluating the output of the ideal transmitter with DPD and pre-gain of (a) PSD: -3 dB, (b) PSD: +5 dB, (c) AM/AM: -3 dB, (d) AM/AM: +5 dB. . . . .	38
4.11	Evaluating the output of the ideal transmitter including pulse shaping filter, DPD and pre-gain of (a) PSD: -3 dB, (b) PSD: +5 dB, (c) AM/AM: -3 dB, (d) AM/AM: +5 dB. . . . .	39
4.12	Frequency response of the pulse shape filter and the inverse pulse shaping filter . . . . .	40

4.13	PSD of the transmitter using a DPD with 265 entries and an ideal pulse shaping compensation filter. . . . .	41
4.14	Variation of the Look-up table size for different pre-gain levels (a) EVM, (b) ACPR. . . .	42
4.15	Variation of the Look-up table size using different interpolation methods for a constant pre-gain of -3 dB (a) EVM, (b) ACPR. . . . .	43
4.16	Identified transmitter without pulse shaping filter using a QMM polynomial with AM/AM order = 7 and AM/PM order = 5, (a) AM/AM, (b) AM/PM. . . . .	45
4.17	Identified transmitter without pulse shaping filter using a MLP with P=9, (a) AM/AM, (b) AM/PM. . . . .	45
4.18	Identified transmitter using a QMM polynomial with AM/AM order = 7 and AM/PM order = 5, (a) AM/AM, (b) AM/PM. . . . .	46
4.19	Identified transmitter using a MLP with P=9, (a) AM/AM, (b) AM/PM. . . . .	46
4.20	Transmitter w/ QMM-polynomial-DPD, $P_{AM/AM} = 7$ , $P_{AM/PM} = 7$ , (a) AM/AM, (b) AM/PM, (c) PSD. . . . .	48
4.21	Frequency response of the identified linear filter of the transmitter (a) with pre-gain = 0 dB, (b) pre-gain = -11 dB, (c) w/o PA. . . . .	49
4.22	Frequency response of the first order of the MP-DPD with P=9, M=2. . . . .	50
4.23	Transmitter w/ pulse shaping filter, w/ and w/o QMM-DPD ( $P_{AM/AM} = 7$ , $P_{AM/PM} = 7$ ), (a) EVM, (b) Mask distance. . . . .	52
4.24	Transmitter w/o pulse shaping filter, w/ and w/o QMM-DPD ( $P_{AM/AM} = 7$ , $P_{AM/PM} = 7$ ), (a) EVM, (b) Mask distance. . . . .	53
4.25	Transmitter w/o pulse shaping filter, w/ and w/o MP-DPD ( $P = 9$ , $M = 2$ ), (a) EVM, (b) Mask distance. . . . .	54

## List of Tables

1.1	Subcarriers per 11ac transmission bandwidth [2]. . . . .	4
1.2	Frequency offsets for spectral requirements [2]. . . . .	4
1.3	Bounds for spectral flatness in 801.11n [2]. . . . .	5
1.4	Allowed relative constellation error in 802.11n [2]. . . . .	5
4.1	Definition of the pseudo-OFDM signal. . . . .	27
4.2	Specification of the QMM PA model. . . . .	30
4.3	Maximal output power for defined PAPR. . . . .	31
4.4	Simulation results of the transmitter (desired output power range in italic). . . . .	32
4.5	Simulation results of the transmitter without pulse shaping filter. (The region where 802.11n is violated is represented italic.) . . . . .	34
4.6	Simulation of the transmitter without PA. . . . .	34
4.7	Simulation results of the transmitter without pulse shaping filter using a DPD with 256 entries. (The region where 802.11n is violated is represented italic.) . . . . .	37
4.8	Simulation results of the transmitter with pulse shaping filter using a DPD with 256 entries. (The region where 802.11n is violated is represented italic.) . . . . .	37
4.9	Simulation results of the transmitter with a DPD using 256 entries and an ideal pulse shaping compensation filter. . . . .	40
4.10	Variation of the Look-up table size for constant pre-gain of -3 dB. . . . .	42
4.11	Identified transmitter without pulse shaping filter using QMM polynomial. . . . .	44
4.12	Identified transmitter without pulse shaping filter using MLP. . . . .	44
4.13	Identified transmitter using QMM polynomial. . . . .	45
4.14	Identified transmitter using a MLP. . . . .	45
4.15	Transmitter w/o and w/ QMM-polynomials-DPD. . . . .	47
4.16	Transmitter w/o and w/ MLP-DPD. . . . .	47
4.17	Identified DPD using a Volterra series with 30 coefficients. . . . .	50
4.18	Transmitter w/o and w/ MP-DPD. . . . .	51
4.19	Transmitter w/o and w/ QMM-polynomial-DPD ( $P_{AM/AM} = 7$ , $P_{AM/PM} = 7$ ) for different pre-gain levels. (The region where 802.11n is violated is represented italic.) . . . . .	52
4.20	Transmitter w/o pulse shaping filter, w/o and w/ QMM-polynomial-DPD ( $P_{AM/AM} = 7$ , $P_{AM/PM} = 7$ ) for different pre-gain levels. (The region where 802.11n is violated is represented italic.) . . . . .	52
4.21	Transmitter without pulse shaping filter, w/o and w/ MP-DPD ( $P = 9$ , $M = 2$ ) for different pre-gain levels. (The region where 802.11n is violated is represented italic.) . . . . .	53
A.1	Possible realizations of a volterra series with order = 9 and 30 independent coefficients. . . . .	57



## Bibliography

- [1] G. Hiertz, D. Denteneer, L. Stibor, Y. Zang, X. Costa, and B. Walke, “The IEEE 802.11 universe,” *IEEE Communications Magazine*, vol. 48, no. 1, pp. 62–70, 2010. [Online]. Available: [http://ieeexplore.ieee.org/xpls/abs\\_all.jsp?arnumber=5394032](http://ieeexplore.ieee.org/xpls/abs_all.jsp?arnumber=5394032)
- [2] IEEE, “Standard: 802.11n-2009,” 2009. [Online]. Available: <http://standards.ieee.org/getieee802/download/802.11n-2009.pdf>
- [3] L. Ward, “802.11ac Technology Introduction, White Paper,” Rohde & Schwarz, Tech. Rep., 2012.
- [4] A. F. Molisch, *Wireless Communications*, ser. Wiley - IEEE. John Wiley & Sons, 2005.
- [5] Y. G. Li and G. L. Stüber, *Orthogonal Frequency Division Multiplexing for Wireless Communications*, ser. Signals and Communication Technology. Springer, 2006.
- [6] L. Smaini, *RF Analog Impairments Modeling for Communication Systems Simulation: Application to OFDM-based Transceivers*. Wiley, 2012.
- [7] B. Bhukania, V. Erceg, J. Zheng, R. Porat, M. Fischer, E. Perahia, V. Jones, and Y. Kim, “11n Spectrum Mask Alignment,” 2011. [Online]. Available: <https://mentor.ieee.org/802.11/dcn/11/11-11-0160-01-000m-11n-spectrum-mask-alignment.ppt>
- [8] E. McCune, *Practical Digital Wireless Signals*, ser. The Cambridge RF and Microwave Engineering Series. Cambridge University Press, 2010.
- [9] J. G. Proakis, *Digital Communications*, 4th ed., ser. McGraw-Hill Series in Electrical and Computer Engineering Series. McGraw-Hill, 2001.
- [10] S. Benedetto and E. Biglieri, *Principles of Digital Transmission: With Wireless Applications*, ser. Information Technology: Transmission, Processing and Storage. Springer, 1999. [Online]. Available: [http://books.google.com/books?hl=en&lr=&id=\\_MZV7fzQmp0C&oi=fnd&pg=PA1&dq=Principles+of+digital+transmission:+with+wireless+applications&ots=XlOnsPojQH&sig=1ElNgPtldP\\_3B7Fo4k4-Gna-cHs](http://books.google.com/books?hl=en&lr=&id=_MZV7fzQmp0C&oi=fnd&pg=PA1&dq=Principles+of+digital+transmission:+with+wireless+applications&ots=XlOnsPojQH&sig=1ElNgPtldP_3B7Fo4k4-Gna-cHs)
- [11] A. S. Tehrani, “Behavioral Modeling of Radio Frequency Transmitters,” Ph.D. dissertation, Chalmers University of Technology, 2009.
- [12] D. Schreurs, M. O’Droma, A. A. Goacher, and M. Gadringer, *RF Power Amplifier Behavioral Modeling*, ser. The Cambridge RF and Microwave Engineering Series. Cambridge University Press, 2009.
- [13] K. M. Gharaibeh, *Nonlinear Distortion in Wireless Systems: Modeling and Simulation with Matlab*, ser. Wiley - IEEE. Wiley, 2012.
- [14] M. Schetzen, *The Volterra and Wiener theories of nonlinear systems*. Krieger Pub., 2006.
- [15] —, “Nonlinear system modeling based on the Wiener theory,” *Proceedings of the IEEE*, vol. 6, no. 12, 1981. [Online]. Available: [http://ieeexplore.ieee.org/xpls/abs\\_all.jsp?arnumber=1456469](http://ieeexplore.ieee.org/xpls/abs_all.jsp?arnumber=1456469)

- [16] S. Benedetto, E. Biglieri, and R. Daffara, “Modeling and Performance Evaluation of Nonlinear Satellite Links-A Volterra Series Approach,” *IEEE Transactions on Aerospace and Electronic Systems*, vol. AES-15, no. 4, pp. 494–507, Jul. 1979. [Online]. Available: <http://ieeexplore.ieee.org/lpdocs/epic03/wrapper.htm?arnumber=4102187>
- [17] V. J. Mathews and G. L. Sicuranza, *Polynomial signal processing*, ser. Wiley series in telecommunications and signal processing. Wiley, 2000.
- [18] A. Tehrani and H. Cao, “A comparative analysis of the complexity/accuracy tradeoff in power amplifier behavioral models,” *Microwave Theory . . .*, vol. 58, no. 6, pp. 1510–1520, 2010. [Online]. Available: [http://ieeexplore.ieee.org/xpls/abs\\_all.jsp?arnumber=5460970](http://ieeexplore.ieee.org/xpls/abs_all.jsp?arnumber=5460970)
- [19] W. Bösch and G. Gatti, “Measurement and simulation of memory effects in predistortion linearizers,” *IEEE Transactions on Microwave Theory and Techniques*, vol. 37, no. 12, pp. 1885–1890, 1989. [Online]. Available: <http://ieeexplore.ieee.org/lpdocs/epic03/wrapper.htm?arnumber=44098>
- [20] G. S. Moschytz and M. Hofbauer, *Adaptive Filter*. Springer-Verlag GmbH, 2000.
- [21] S. S. Haykin, *Adaptive filter theory*, ser. Prentice-Hall information and system sciences series. Prentice Hall, 2002.
- [22] C. B. Moler, *Numerical Computing with Matlab*. Society for Industrial and Applied Mathematics, 2004. [Online]. Available: <http://books.google.at/books?id=-vPtcrifH0C>
- [23] E. Powers, “A new Volterra predistorter based on the indirect learning architecture,” *IEEE Transactions on Signal Processing*, vol. 45, no. 1, pp. 223–227, 1997. [Online]. Available: <http://ieeexplore.ieee.org/lpdocs/epic03/wrapper.htm?arnumber=552219>
- [24] H. Schmid, “How to use the FFT and Matlab ’ s pwelch function for signal and noise simulations and measurements,” University of Applied Sciences and Arts Northwestern Switzerland, Institute of Microelectronics, Tech. Rep. August, 2012. [Online]. Available: <http://www.fhnw.ch/technik/ime/publikationen/2012/how-to-use-the-fft-and-matlab2019s-pwelch-function-for-signal-and-noise-simulations-and-measurements>
- [25] F. Harris, “On the use of windows for harmonic analysis with the discrete Fourier transform,” *Proceedings of the IEEE*, vol. 66, no. 1, pp. 51–83, 1978. [Online]. Available: <http://ieeexplore.ieee.org/lpdocs/epic03/wrapper.htm?arnumber=1455106>
- [26] F. Ghannouchi and O. Hammi, “Behavioral modeling and predistortion,” *Microwave Magazine, IEEE*, no. December, 2009. [Online]. Available: [http://ieeexplore.ieee.org/xpls/abs\\_all.jsp?arnumber=5259211](http://ieeexplore.ieee.org/xpls/abs_all.jsp?arnumber=5259211)
- [27] C. Yu, L. Guan, E. Zhu, and A. Zhu, “Band-Limited Volterra Series-Based Digital Predistortion for Wideband RF Power Amplifiers,” vol. 60, no. 12, pp. 4198–4208, 2012. [Online]. Available: [http://ieeexplore.ieee.org/xpls/abs\\_all.jsp?arnumber=6353238](http://ieeexplore.ieee.org/xpls/abs_all.jsp?arnumber=6353238)
- [28] B. Shi, W. Shan, and L. Sundstmm, “Effects of Look-Up Table Size on Adaptive Predistortion Linearizer Systems with Error Sources,” pp. 1231–1234, 2003.